Molecular motor function in axonal transport in vivo probed by genetic and computational analysis in *Drosophila*

Gerald F. Reis[a,b,c,*,†], Ge Yang[d,*,‡], Lukasz Szpankowski[a,e,f], Carole Weaver[a,c], Sameer B. Shah[c,g], John T. Robinson[h], Thomas S. Hays[h], Gaudenz Danuser[d,§], and Lawrence S. B. Goldstein[a,c,f]

[a]Howard Hughes Medical Institute, [b]Neuroscience Graduate Program, and [c]School of Medicine, University of California, San Diego, La Jolla, CA 92093; [d]Department of Cell Biology, Scripps Research Institute, La Jolla, CA 92037; [e]Bioinformatics and Systems Biology, Department of Bioengineering, University of California, San Diego, La Jolla, CA 92093; [f]Department of Cellular and Molecular Medicine, University of California, San Diego, La Jolla, CA 92093; [g]Fischell Department of Bioengineering, University of Maryland, College Park, MD 20742; [h]Department of Genetics, Cell Biology and Development, University of Minnesota, Minneapolis, MN 55455

ABSTRACT **Bidirectional axonal transport driven by kinesin and dynein along microtubules is critical to neuronal viability and function. To evaluate axonal transport mechanisms, we developed a high-resolution imaging system to track the movement of amyloid precursor protein (APP) vesicles in *Drosophila* segmental nerve axons. Computational analyses of a large number of moving vesicles in defined genetic backgrounds with partial reduction or overexpression of motor proteins enabled us to test with high precision existing and new models of motor activity and coordination in vivo. We discovered several previously unknown features of vesicle movement, including a surprising dependence of anterograde APP vesicle movement velocity on the amount of kinesin-1. This finding is largely incompatible with the biophysical properties of kinesin-1 derived from in vitro analyses. Our data also suggest kinesin-1 and cytoplasmic dynein motors assemble in stable mixtures on APP vesicles and their direction and velocity are controlled at least in part by dynein intermediate chain.**

Monitoring Editor
Yixian Zheng
Carnegie Institution

Received: Dec 9, 2011
Revised: Feb 21, 2012
Accepted: Mar 2, 2012

This article was published online ahead of print in MBoC in Press (http://www.molbiolcell.org/cgi/doi/10.1091/mbc.E11-11-0938) on March 7, 2012.

*These authors contributed equally to this work.

Present addresses: †Department of Pathology, University of California, San Francisco, San Francisco, CA 94143; ‡Department of Biomedical Engineering and Lane Center for Computational Biology, Carnegie Mellon University, Pittsburgh, PA 15213; §Harvard Medical School, Boston, MA 02115.

Address correspondence to: Lawrence S. B. Goldstein (lgoldstein@ucsd.edu) and Gaudenz Danuser (Gaudenz_Danuser@hms.harvard.edu).

Abbreviations used: APP, amyloid precursor protein; APPYFP, yellow fluorescent protein–tagged amyloid precursor protein; DHC, dynein heavy chain; DIC, dynein IC; DLC, dynein light chain; EB1-GFP, green fluorescent protein–tagged EB1; EGTA, ethylene glycol tetraacetic acid; GEN, genomic; GST, glutathione *S*-transferase; KHC, kinesin heavy chain; KLC, kinesin light chain; LUV, light ultraviolet cleavage fragment; NA, numerical aperture; PNS, postnuclear supernatant; RNAi, RNA interference; SG26.1 Gal4, Gal4 gene enhancer trap strain; SYT, synaptotagmin; SYTGFP, green fluorescent protein–tagged synaptotagmin; UAS, upstream activation sequence.

INTRODUCTION

A hallmark of the neuron is its polarized axon, which can extend for more than 1 m in humans. Within the axon, a wide variety of cargoes essential for the viability and function of the neuron must be transported along microtubules between the neuronal cell body and synapses (Grafstein and Forman, 1980). Understanding how molecular motor proteins drive this axonal transport is important to the understanding of a wide range of neurological diseases (Goldstein, 2003; Stokin and Goldstein, 2006; Chevalier-Larsen and Holzbaur, 2006; De Vos *et al*., 2008).

Axonal transport toward synapses (anterograde transport) is driven by microtubule plus end–directed kinesins, especially those from the kinesin 1–4 and 13 families (Goldstein and Yang, 2000; Lawrence *et al*., 2004; Hirokawa and Takemura, 2005). Transport toward the neuronal cell body (retrograde transport) is driven by microtubule minus end–directed cytoplasmic dynein (King, 2000; Vallee *et al*., 2004). Much information about the biochemical and mechanical mechanisms of kinesin-1 and cytoplasmic dynein movement has emerged from in vitro studies. For example, single

kinesin-1 motors move toward microtubule plus ends for hundreds of nanometers (Howard *et al.*, 1989; Block *et al.*, 1990; Svoboda *et al.*, 1993). Consistent with this high degree of processivity, the velocity of microtubule or bead movement driven by kinesin-1 does not vary with the number of available motors (Howard *et al.*, 1989; Block *et al.*, 1990; Svoboda *et al.*, 1993). In vitro bead movement generated by cytoplasmic dynein is also processive (Wang *et al.*, 1995; Reck-Peterson *et al.*, 2006; Gennerich *et al.*, 2007), though to a lesser extent than kinesin-1, and is enhanced by dynactin (Schroer, 2004).

It remains largely unknown to what extent the in vitro data predict in vivo motor behavior. Indeed, some of the in vitro characteristics seem at odds with in vivo observations of motor-driven vesicle and organelle motion. First, movement of single cargoes is often substantially faster in vivo than movement supported by single or multiple kinesin-1 and cytoplasmic dynein motors in vitro (Kural *et al.*, 2005). Second, distances traveled by cargoes in vivo can be severalfold longer than the average run lengths of kinesin-1 and cytoplasmic dynein motors in vitro (Block *et al.*, 1990; Wang and Sheetz, 2000; Kim *et al.*, 2007). In addition, cargoes in vivo can switch frequently between anterograde and retrograde movement (Gross, 2004). Thus comprehensive in vivo analysis of cargo motion is essential to understanding the mechanisms of kinesin and dynein function in axonal transport.

Previous studies of vesicle and organelle transport in vivo relied on experimental models lacking most to all motor function or high-level overexpression of kinesin-1, cytoplasmic dynein, or dynactin subunits (Gindhart *et al.*, 1998; Martin *et al.*, 1999; Boylan and Hays, 2002). These manipulations often caused pleiotropic phenotypes, thus providing limited information as to how the kinetics of movement depend on specific motor properties. To circumvent these problems, we used mild, well-defined genetic reduction or overexpression of functional kinesin-1, cytoplasmic dynein, or dynactin subunits. To achieve sufficient sensitivity for robust interpretation of the resulting weak phenotypes, we developed computer-assisted quantification of the behavior of large numbers of amyloid precursor protein (APP) axonal vesicles. The axonal transport of APP is of significant interest, owing to its likely involvement in the development of Alzheimer's disease, known vesicular properties, and fast axonal transport (Kamal *et al.*, 2000, 2001; Stokin *et al.*, 2005; Stokin and Goldstein, 2006; Duncan and Goldstein, 2006). Our focus on kinesin-1, as opposed to other members of the kinesin superfamily, is based on previous work showing that APP transport is abolished in the absence of kinesin-1 (Ferreira *et al.*, 1992; Amaratunga *et al.*, 1995; Yamazaki *et al.*, 1995; Kaether *et al.*, 2000) and that APP can associate with kinesin-1 either directly via interactions with the C-terminus domain of the light chain of kinesin-1 (Kamal *et al.*, 2000; Gunawardena and Goldstein, 2001) or indirectly through cytosolic adaptor proteins, such as the JNK-interacting protein 1 (Inomata *et al.*, 2003; Matsuda *et al.*, 2003). Combined with statistical analyses of the distribution of motion parameters, the experimental approach described here allowed us to test different models of motor interaction in vivo.

RESULTS

Establishing the properties of axonal APP vesicle movement in vivo

We probed the transport behavior of individual APP vesicles in vivo by using SG26.1 Gal4 (Gal4 gene enhancer trap strain) to drive the expression of UAS-APPYFP in *Drosophila*. Because the expression of SG26.1 Gal4 is confined to a subset of ventral ganglion neurons, APPYFP movement could be tracked with single-axon resolution within segmental nerves. Analysis of green fluorescent protein–tagged EB1 (EB1-GFP) transport in these neurons confirmed that movement away from cell bodies is microtubule plus end–directed and anterograde (Supplemental Figure S1A), consistent with a previous report (Stone *et al.*, 2008). Using high spatial (0.126 micron) and temporal (10 Hz) resolution imaging, we characterized the movement of APP in an otherwise wild-type background (Figures 1, A–E, and S1, A–F, and Supplemental Movie S1; see *Materials and Methods*): 32.3% of the vesicles moved anterogradely and 18.2% moved retrogradely (Figure 1, A–C), whereas 40.4% were stationary and 9.1% reversed direction with an average switch frequency of 6.09 switches/min (Figures 1C and S1B). Switches generally did not involve pausing, consistent with a previous report of lipid droplet movement in *Drosophila* embryos (Welte *et al.*, 1998). Thus directional switches are mediated by an apparently instantaneous change in the balance of active motors.

Anterograde velocities of APP vesicles depend on the amount of kinesin-1

Considerable evidence demonstrates that APP movement is driven by kinesin-1 (Koo *et al.*, 1990; Ferreira *et al.*, 1992; Amaratunga *et al.*, 1993; Simons *et al.*, 1995; Tienari *et al.*, 1996; Kamal *et al.*, 2000; Szodorai *et al.*, 2009). We observed that a substantial fraction of APPYFP vesicles traveled at velocities faster than those observed for kinesin-1 motors in vitro, up to a maximum of 2.85 µm/s (Figure 1D), consistent with previous reports (Kaether *et al.*, 2000; Stamer *et al.*, 2002; Goldsbury *et al.*, 2006).

Kinesin-1-driven movement in vivo, which is substantially faster than in vitro, may be related to a different regulation of the ATPase cycle in vivo. Alternatively, multiple kinesin motors may coordinate to generate faster velocities, as speculated by Kural and colleagues (Kural *et al.*, 2005). The latter would be incompatible with the independence of velocity and motor number for kinesin-1 seen in vitro (Howard *et al.*, 1989; Block *et al.*, 1990; Spudich, 1990). Additionally, it would be inconsistent with more recent in vivo data of lipid droplet movement in *Drosophila* embryos, which suggest that neither velocity nor run length changes significantly with varying amounts of kinesin-1 (Shubeita *et al.*, 2008).

To test the hypothesis that the velocities and run lengths of APP vesicles may be determined by the amount of kinesin-1, we performed genetic, biochemical, and statistical analyses to correlate the number of active kinesin-1 molecules with vesicle behavior. We tested four predictions made by this hypothesis. A first prediction is that the anterograde velocity distribution should be nonnormal with multiple modal peaks reflecting differential occupancy of active motors. We tested this possibility by statistical mode analysis (Fraley and Raftery, 2002) and found that the distribution was best fit by three modes (Figure 1E; see *Materials and Methods*). Thus the first prediction is fulfilled. Interestingly, multimodal cargo velocity distributions have been reported previously in motility assays under substantial mechanical load of viscoelastic drag and in intracellular transport of PC12 cells and *Xenopus* melanophores (Hill *et al.*, 2004; Levi *et al.*, 2006; Gagliano *et al.*, 2010).

A second prediction is that increased velocities should correlate with increased run lengths (or reduced pause frequency; Spudich, 1990). Because our relatively short observation window of 15 s leads to truncation of run length for many vesicles (Figure S1C), we tested for a correlation of segmental velocity with pause frequency (see Supplemental Material). For controls, the anterograde correlation coefficient was –0.45, indicating that the faster the cargo, the lower

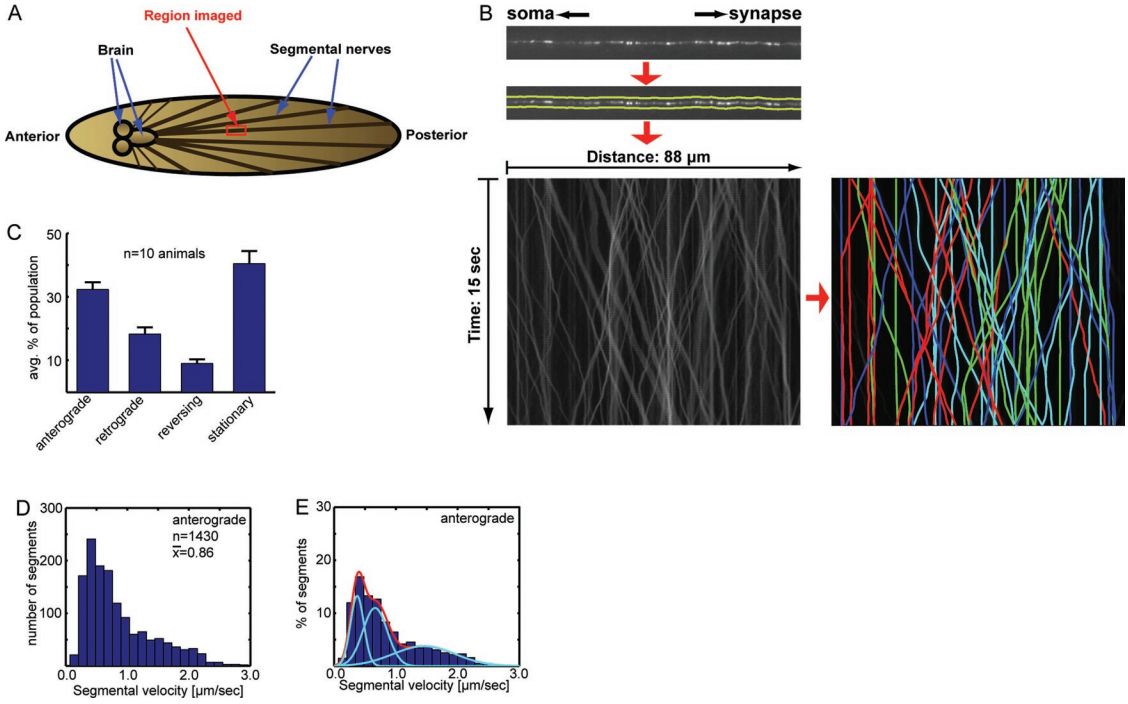

FIGURE 1: Characterization of the properties of APPYFP transport in *Drosophila* segmental nerve axons in vivo. (A) In vivo data were collected from an axonal region ~900 µm from the cell body (imaging field size: 88 µm in length). A standard data set consisted of four video segments of 15-s duration recorded for 10 individual animals. (B) Top panel, first frame of a time-lapse sequence showing APPYFP transport. Middle panel, a band (5 pixels in thickness) flanking the axon is extracted from each frame. Bottom, left panel, bands from all frames are pasted top-to-bottom to form a kymograph. Bottom, right panel, computationally recovered vesicle trajectories color-coded and overlaid on the kymograph; colors were selected randomly to differentiate crossing trajectories. Truncated vesicle trajectories were excluded for each movie. (C) Classification of vesicle trajectories (total number of trajectories = 1890; all error bars show SEM): anterograde, 32.3% ± 2.3%; retrograde, 18.2% ± 2.1%; stationary, 40.4% ± 4.0%; reversing, 9.1% ± 1.2%. (D) Distribution of anterograde segmental velocities. Although the mean segmental velocity was 0.86 µm/s, the distribution of segmental velocities had a long tail toward higher values, with 41% of vesicles moving faster than 0.8 µm/s and 13% moving faster than 1.6 µm/s (maximal anterograde segmental velocity was 2.85 µm/s). (E) The distribution of anterograde segmental velocities has three distinct modes (cyan), with centers increasing as multiples (based on fit): mode 1, ~0.4 µm/s; mode 2, ~0.8 µm/s (2×); and mode 3, 1.6 µm/s (4×). See Table S1 for a definition of exact mode centers, spreads, and fractions of segment population. Superposition of all three modes is shown in red.

the average probability of a pause. Thus the second prediction is also fulfilled.

A third prediction is that reducing the amount of kinesin-1 on vesicles should shift the distribution of velocities to lower modes without changing the mode centers. We tested this possibility by partially reducing kinesin-1 level, thereby circumventing the issues of organismal lethality and cellular defects reported in previous in vivo studies (Gindhart *et al.*, 1998; Hurd and Saxton, 1996; Boylan and Hays, 2002). We used two null point mutation alleles for kinesin heavy chain (KHC), khc^{8} and khc^{20} (Saxton *et al.*, 1991; Brendza *et al.*, 2000), and one deletion allele for kinesin light chain (KLC), klc^{8ex94} (Gindhart *et al.*, 1998). Western blot analysis of kinesin-1 heterozygotes (see *Materials and Methods*) confirmed that the removal of one functional *khc* or *klc* gene caused ~50% reduction in KHC or KLC proteins (Figure 2, A–C). Interestingly, *khc* reduction also resulted in KLC protein reduction, whereas *klc* reduction did not affect KHC protein levels. Thus KLC protein levels appear to depend on KHC but not vice-versa, consistent with previous work in *Drosophila* S2 cells (Ligon *et al.*, 2004).

To test whether kinesin-1 reduction translates to less motor protein assembly on vesicles, we used bottom-loaded sucrose flotation step gradients (see *Materials and Methods*). In our experimental design, a fraction at the interface of the 8/35 sucrose step consists of floated membranes and vesicles. We found that 50% *khc* gene reduction leads to ~50% reduction in both KHC and KLC proteins in the 8/35 fraction (Figure 2, D and E), indicating that *khc* reduction leads to less kinesin-1 associated with vesicles. Under these conditions, we observed substantial decreases in anterograde APPYFP velocities (Figures 2F and S2A). Although the distributions were best fit by three modes (as in control), there were significant shifts in the relative contribution of each mode in kinesin-1 reductions (Figures 2, G and H, and S5B and Supplemental Table S1). Moreover, either *khc* or *klc* reduction led to significantly shorter run lengths, increased pause frequency, increased pause duration, and a larger fraction of stationary vesicles (Figure S2, B–H). Together these biochemical and genetic findings are consistent with the notion that the number of functional kinesin-1 motors assembled per cargo is reduced with kinesin-1 reduction, causing a decrease in the anterograde velocity and a shift in the occupancy of modal velocities (unlike lipid droplet transport in *Drosophila* embryos [Shubeita *et al.*, 2008]).

A fourth prediction of the hypothesis that the velocities of APP vesicles may be determined by the amount of kinesin-1 is that the correlation of anterograde velocity and pause frequency should be preserved in kinesin-1 reduction. Indeed, the magnitude of the

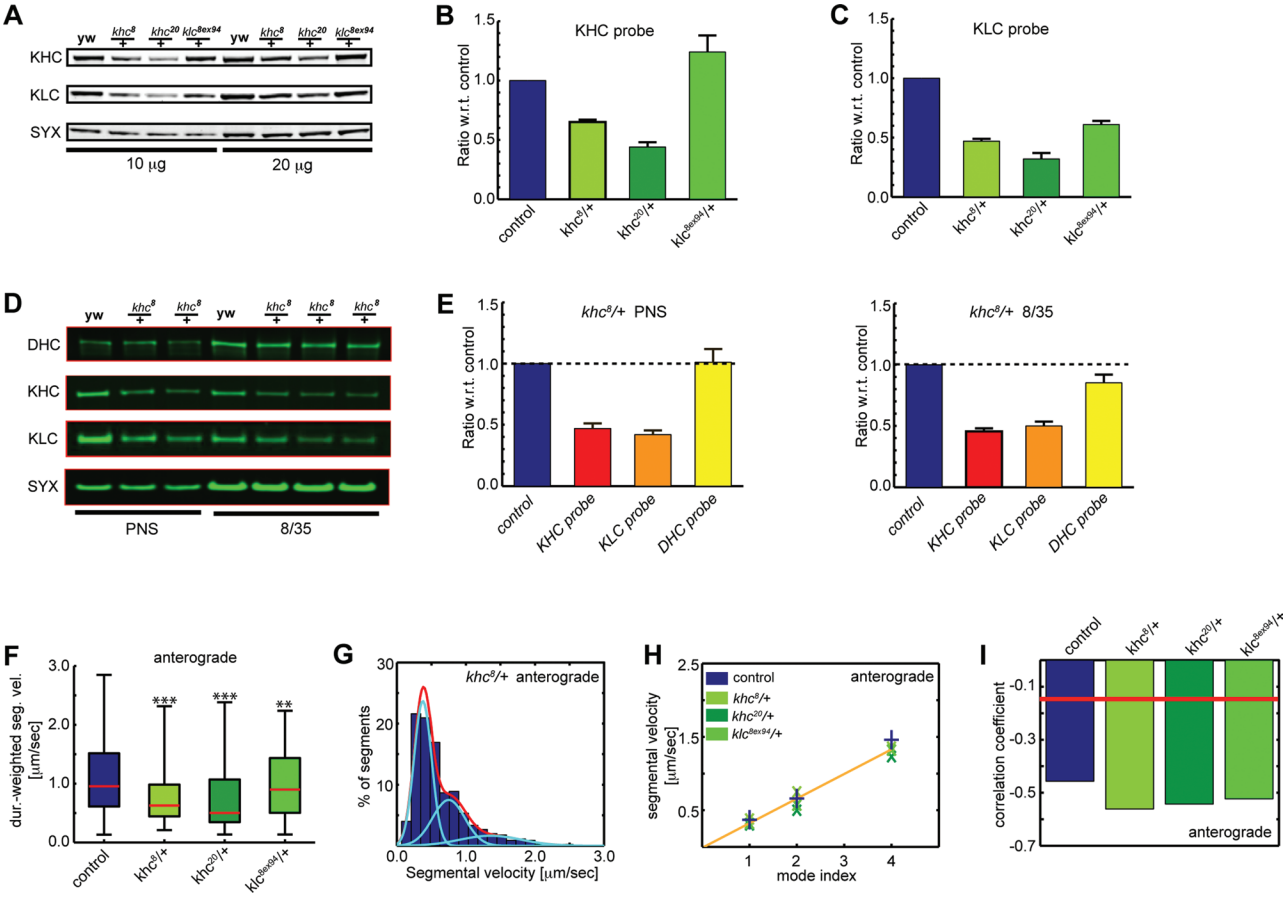

FIGURE 2: Anterograde APPYFP velocities are relatively stable over time and depend on kinesin-1 amounts. (A–C) Western blot analysis in animals heterozygous for null mutations in *khc* or *klc* subunits of kinesin-1: khc^{8}/+, khc^{20}/+, and klc^{8ex94}/+ (syntaxin is used as a loading control). Reduction of *khc* leads to both KHC and KLC protein reduction; reduction of *klc* leads to reduction in KLC protein only (n = 4 for each condition). (D) Western blot analysis of membrane-bound KHC, KLC, and DHC proteins in khc^{8}/+. (E) Reduction in *khc* leads to decrease in membrane-bound KHC and KLC levels without significantly affecting membrane-bound DHC. PNS, postnuclear supernatant fraction; 8/35, vesicular fraction. (F) Anterograde duration-weighted segmental velocities (average velocity behavior that vesicles exhibit per time spent moving) for control and kinesin-1 reduction genotypes (mean μm/s ± SD): control, 1.09 ± 0.58; khc^{8}/+, 0.77 ± 0.44; khc^{20}/+, 0.71 ± 0.48; klc^{8ex94}/+, 0.96 ± 0.52. Box plots outline distribution of segmental velocities for each genotype. The red line indicates the median of the data. Upper and lower box edges represent 75 percentile and 25 percentile of the data, respectively. Upper and lower whiskers represent maximum and minimum of the data, respectively. Notation for p values: *, $p < 0.05$; **, $p < 0.01$; ***, $p < 0.001$. (G) As in control, anterograde unweighted segmental velocity distribution of khc^{8}/+ has three modes (cyan; red line: superposition of modes). However, in khc^{8}/+, there is a significant increase in the population of cargoes in mode 1 (slowest mode) from ~26% in control up to 54% in khc^{8}/+, mostly at the expense of vesicles in mode 3 (fastest mode; 34% in control down to 13% in khc^{8}/+); see Figure S5B for an overlay of control and khc^{8}/+ mode analysis. Other kinesin-1 reduction genotypes showed similar behavior (see Table S1). (H) Linear regression of anterograde velocity mode centers assembled for kinesin-1 reduction genotypes (centers follow approximately a 1:2:4 ratio). (I) Negative correlation coefficients between velocity and pause frequency demonstrating weakly processive behavior of kinesin-1–driven APP vesicle transport. Red bar shows 99% range (3σ) in the correlation of random pairings drawn from the same distributions of velocities and pause frequencies (see Supplemental Material).

correlation coefficients for all kinesin-1 reduction genotypes was in the range of –0.45 to –0.55, which is statistically highly significant (Figure 2I; see Supplemental Material). Thus all four predictions are fulfilled.

A potential concern is whether kinesin-1 reduction causes nonspecific global toxicity to axonal transport, including swellings, "organelle jams," and blockage in transport (Hurd and Saxton, 1996; Martin *et al.*, 1999; Gunawardena and Goldstein, 2001; however, see Pilling *et al.*, 2006). Several observations suggest nonspecific global toxicity is an unlikely explanation for our data. First, there was no organismal phenotype characteristic of axonal transport defects, such as a tail-flip phenotype or animal inviability. Second, while axonal swellings were present in our kinesin-1 reduction genotypes, they were generally found in distal axonal regions, rather than in the more proximal region we analyzed. Third, nonselective poisoning would likely shift modal velocity values, whereas we observed fractional shifts in mode. Fourth, both kinesin-1–dependent and kinesin-1–independent transport would be expected to show impairment. To test the latter possibility, we analyzed the movement of synaptotagmin (SYT)—a kinesin-3 cargo (Yonekawa *et al.*, 1998; Pack-Chung *et al.*, 2007) tagged with GFP (SYTGFP), in khc^{8}/+ and klc^{8ex94}/+ animals. As expected, we observed that kinesin-1 reduction

does not significantly change the total number of SYTGFP moving vesicles (see Figure 4I later in the paper) or the population percentages (Figure S6, G–J; see also Table S2). Furthermore, kinesin-1 reduction has no significant effect on retrograde velocity (Figure S6, B and D) or anterograde run length (Figure S6E). Although we observed a mildly significant decrease in anterograde segmental velocity for *khc*^{8}/+, this was not seen in *klc*^{8ex94}/+ (Figure S6, A and C). Interestingly, a significant increase in retrograde run length was noted (Figure S6F), which may relate to the overall decrease in kinesin-1 related transport. Taken together, the SYTGFP data suggest that nonspecific global toxicity is an unlikely mechanism underlying the effects of kinesin-1 reduction on APP movement.

Kinesin-1–driven anterograde velocity modes are relatively stable

Current models of vesicle movement make different predictions about the stability of movement behavior during axonal transport. For example, models in which motor proteins actively associate and dissociate with vesicles to determine directionality predict that certain parameters will vary over time (e.g., before and after pauses). Alternatively, models that invoke stable loading of vesicles in neuronal cell bodies predict substantial stability of movement before or after pauses and during runs. In fact, a prediction of the hypothesis that varying kinesin-1 motor amounts on APP vesicles control their behavior is that while the distribution of velocities is broad, the velocity of any given vesicle should remain relatively stable if motor number does not change over time. Hence, we analyzed movement behaviors relative to pauses and run lengths.

Our measurements of pause frequency indicate that APP vesicles pause infrequently during movement (Figure S1, D–E). Consistent with this, the observed average run length for APPYFP vesicles was 7.63 μm (Figure S2B), severalfold higher than in vitro (Howard *et al.*, 1989; Block *et al.*, 1990). Because our cargo trajectories are truncated spatially and temporally, even this value is too low. Our calculated estimated bulk anterograde run length is 11.7 μm (see Supplemental Material). Indeed, longer-duration movies (2 min of continuous imaging) generated an average run length of 21.85 μm (SEM = 2.3 μm; n = 47 segments; unpublished data).

We also probed the stability of APP movement by calculating the probability that a vesicle changes velocity mode during runs and after pauses and comparing it with random changes (see Supplemental Material). Consistent with the idea of stable motor loading for APP axonal transport, we found that APP velocity modes are relatively stable.

Kinesin-1 reduction impairs retrograde transport

To examine the effects of kinesin-1 reduction on the retrograde transport of APP, we first determined the retrograde behavior of APPYFP vesicles under control conditions. The observed mean retrograde segmental velocity was 0.87 μm/s (Figure 3A), similar to values reported for cytoplasmic dynein in vitro (King and Schroer, 2000; Reck-Peterson *et al.*, 2006). However, retrograde segmental velocity distribution showed three modes, with velocities as high as 3.14 μm/s (Figure 3B and Table S1). As with anterograde transport, retrograde velocities showed high modal stability (Figure 3E). The observed retrograde run length was 7.08 μm (Figure S2J), and the calculated bulk retrograde run length was 13.2 μm. Longer-duration recordings confirmed the longer calculated retrograde run length (mean = 14.18 μm; SEM = 2.7 μm; n = 26 segments; 2 min of imaging; unpublished data).

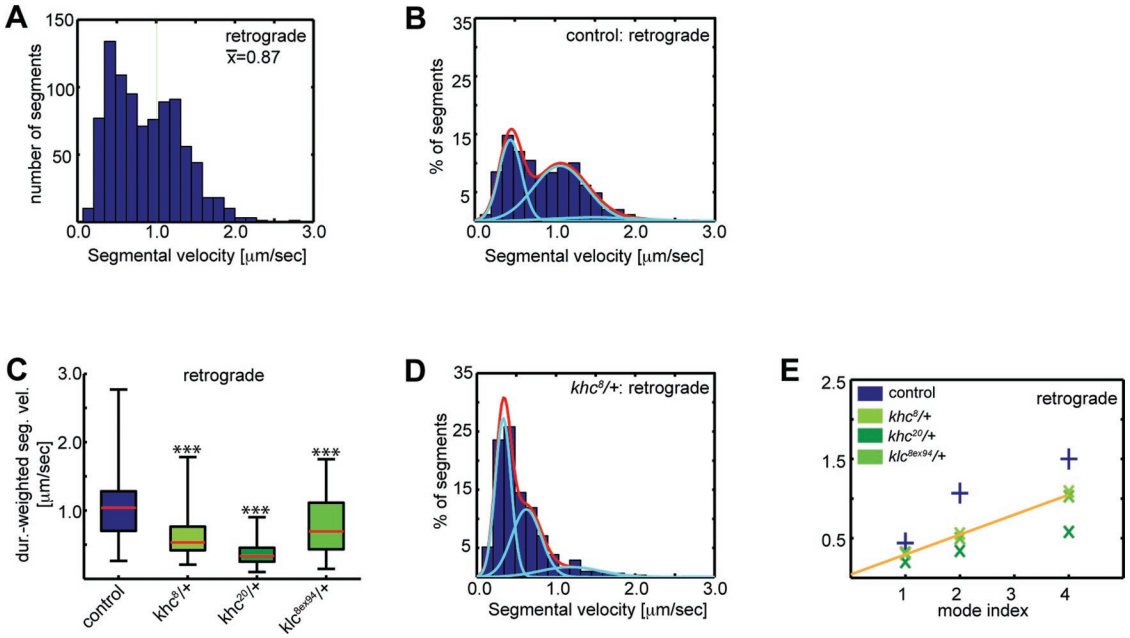

FIGURE 3: Kinesin-1 reduction leads to impairment in retrograde APPYFP transport. (A) Distribution of retrograde segmental velocities. (B) Retrograde unweighted segmental velocity mode analysis for control shows three modes (cyan); see Table S1 for a definition of mode centers, spreads, and fractions of segment population. Superposition of modes is shown in red. (C) Analysis of retrograde duration-weighted segmental velocities shows a significant decrease in mean velocity for kinesin-1 reduction genotypes (mean μm/s ± SD): control, 1.02 ± 0.41; *khc*^{8}/+, 0.65 ± 0.36; *khc*^{20}/+, 0.37 ± 0.19; *klc*^{8ex94}/+, 0.76 ± 0.39. (D) Decomposition of retrograde segmental velocity distribution into three modes for *khc*^{8}/+. Although the centers of the three modes are similar to control conditions (compare with B), there is a significant shift of the vesicle population into mode 1 (see also Table S1). Red line, superposition of modes. A similar phenomenon is observed for *khc*^{20}/+ and *klc*^{8ex94}/+ (see Table S1). (E) Linear regression of retrograde velocity mode centers assembled for kinesin-1 reduction genotypes follows a ratio of ~1:2:4.

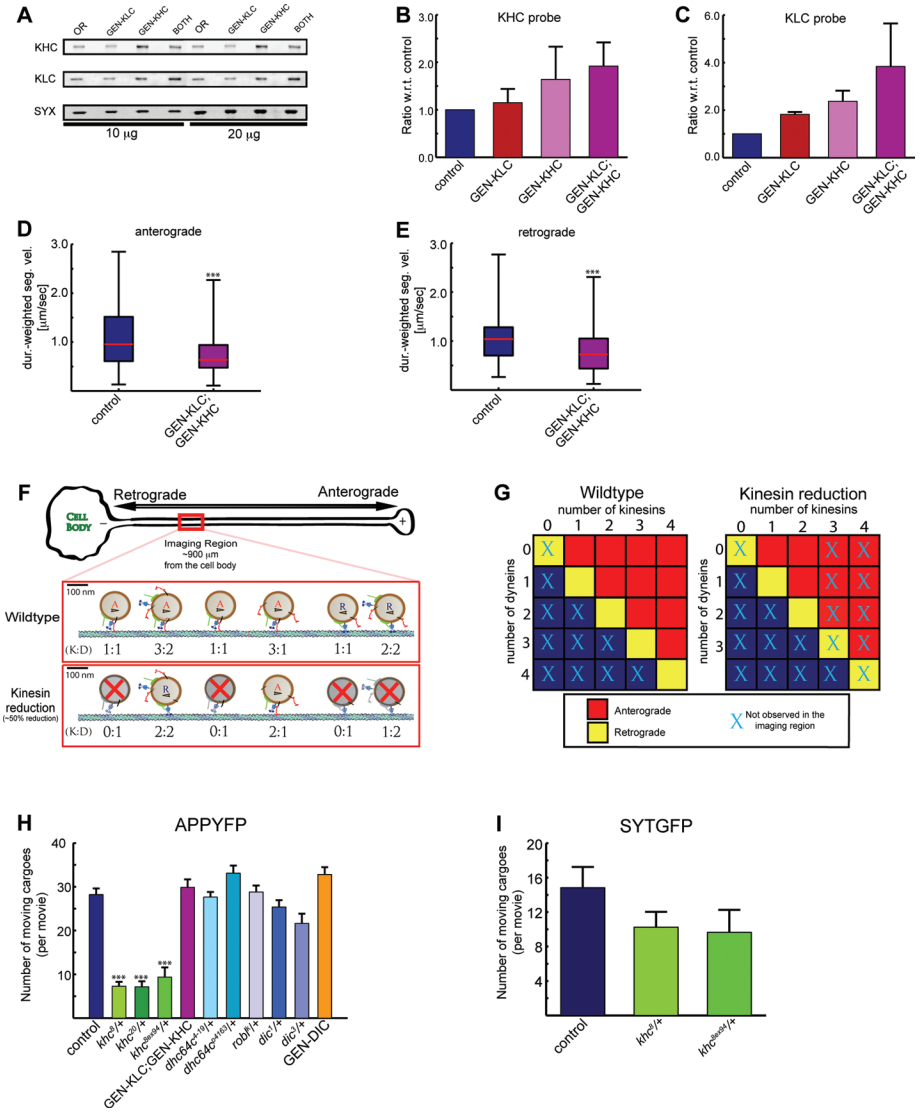

FIGURE 4: Kinesin-1 overexpression and reduction experiments suggest that the impairment of APPYFP retrograde transport seen in kinesin-1 reduction may result from a sampling bias. (A–C) Western blot analysis of kinesin-1 proteins in *khc* and *klc* overexpression genotypes (GEN-KHC and GEN-KLC): GEN-KHC showed increase in both KHC and KLC proteins by ~50–100%, whereas only KLC protein was increased by 50–100% in GEN-KLC. Simultaneous overexpression of *khc* and *klc* led to nearly 100% increase in KHC protein and a much higher (~300%) increase in KLC protein. Thus KLC protein levels appear to depend on KHC but not vice versa (n = 4 for each condition). (D and E) Kinesin-1 overexpression leads to a significant reduction in both anterograde and retrograde duration-weighted segmental velocities (mean µm/s ± SD). Anterograde: control, 1.09 ± 0.58; GEN-KLC;GEN-KHC, 0.78 ± 0.46; retrograde: control, 1.02 ± 0.41; GENKLC;GEN-KHC, 0.78 ± 0. (F) Schematic model for the sampling bias in kinesin-1 reduction (imaged region highlighted in red). Top panel, hypothetical distribution of moving vesicles in control. Vesicles with a number of active kinesins equal to or greater than the number of active dyneins (K:D = 1 and K:D > 1) are far more likely to enter the axon and reach the imaged region compared with vesicles with a surplus of active dynein motors (K:D < 1). Because kinesin-1 reduction may lead to an increase in the vesicle population, with K:D < 1, vesicles are more likely to leave the imaged region and return to the cell body (crossed-out vesicles). Hence, vesicles reaching the imaged region would have fewer dynein motors compared with control, resulting in an apparent defect in retrograde transport. (G) The sampling phenomenon proposed in (G) can be formalized by a matrix of motor combinations per vesicle. Only combinations in the upper triangle (K:D > 1) and on the diagonal (K:D = 1) would enter the axon and reach the imaged region. Vesicles in the lower triangle (K:D < 1) would escape observation. (H) A marked decrease in total moving APPYFP cargoes is observed when kinesin-1 is reduced (all error bars show SEM; see Table S1). (I) Kinesin-1 reduction does not significantly alter the total number of moving SYTGFP cargoes (all error bars show SEM; see Table S2).

Reduction in *khc* and *klc* gene dosage led to substantial impairment in retrograde transport. We found significant decreases in APPYFP segmental velocities (Figures 3C and S2I) and a major shift in occupancy (but not value) of velocity modes (Figures 3, D and E, and S5F and Table S1). In addition, there was a significant decrease in retrograde run lengths and significant increases in retrograde pause frequencies and durations (Figure S2, J–L). Thus kinesin-1 plays an important role in bidirectional transport, as proposed previously (Brady *et al.*, 1990; Martin *et al.*, 1999; Pilling *et al.*, 2006; Kim *et al.*, 2007; Colin *et al.*, 2008). Although *khc* reductions produced more pronounced effects compared with *klc*, we observed that both subunits play a similar role, unlike previous work in which only KHC had a significant contribution (Ling *et al.*, 2004).

We considered three explanations for the impairment in retrograde transport by kinesin-1 reduction: dynein vesicle loading, motor activation, and sampling bias.

If loss of kinesin-1 leads to reduced loading of cytoplasmic dynein on APP vesicles, as proposed previously (Ally *et al.*, 2009), we should see evidence for this in our flotation assay. However, we noted that dynein heavy chain (DHC) protein levels in khc^{8}/+ remained unchanged in the postnuclear supernatant (PNS) and exhibited only a minor (15%) decrease in the 8/35 fraction (Figure 2, D and E). Thus loss of kinesin-1 does not appear to significantly lower the amounts of cytoplasmic dynein on floated vesicles.

The hypothesis of dynein activation by kinesin (Ally *et al.*, 2009) cannot be tested directly in our system. However, a prediction of this hypothesis is that kinesin overexpression will lead to increased dynein activation. Thus we overexpressed *khc*, *klc*, or both together (see *Materials and Methods*) and analyzed APPYFP movement. Western blot analysis confirmed the expected increase in KHC and KLC proteins in kinesin-1 overexpression genotypes (Figure 4, A–C). Movement analysis in these backgrounds showed a significant impairment in retrograde transport, with decreases in segmental velocities and run lengths, as well as increases in pause frequency and duration (Figures 4E and S2, I–L). These findings do not support the hypothesis that kinesin-1 activates cytoplasmic dynein. Intriguingly, we also observed a significant impairment in anterograde transport (Figures 4D and S2, A–D), even though there was a significant increase in the anterograde population fraction (Figure S2F).

Sampling bias attributes the observed impairment in retrograde transport to an

overall reduction in APP movement. The bias would result from fewer axonal retrograde vesicles within the observation window, resulting in an apparent inhibition of retrograde transport (Figure 4, F and G). Indeed, we observed a significant decrease in the total number of APPYFP vesicles in kinesin-1 reductions, an effect we observed for no other genotype (Figure 4H). Thus sampling bias alone may explain the apparent impairment of retrograde transport upon reduction of kinesin-1.

Reduction of cytoplasmic dynein and dynactin subunits confirms modal stability is a generic feature of kinesin-1–driven APP transport

Previous work in *Drosophila* embryos showed that impairment to DHC or the p150 subunit of dynactin disrupts anterograde movement (Gross *et al.*, 2002). From this, dynactin emerged as a potential coordinating factor. Other work has proposed that dynactin promotes dynein attachment to vesicles and enhances retrograde motor processivity through p150 binding to microtubules (Karki and Holzbaur, 1999; King and Schroer, 2000; Schroer, 2004). However, more recent work demonstrated that cargo motility in vivo does not require p150 microtubule binding (Kim *et al.*, 2007). In addition, loss of dynactin does not prevent dynein association with vesicles (Haghnia *et al.*, 2007). Although disruption of the dynactin complex via *arp1* deletion or *p50* overexpression led to bidirectional impairment in axonal transport (Haghnia *et al.*, 2007; Kwinter *et al.*, 2009), the severity of the effects raised concerns about the specificity of the inhibition. Thus we further probed models of motor protein coordination and attachment by evaluating the effects of reduction in cytoplasmic dynein and dynactin on APP transport (see *Materials and Methods*). For cytoplasmic dynein, we studied two null point mutation alleles for DHC, $dhc64c^{p4163}$ and $dhc64c^{4-19}$ (see *Materials and Methods*), two null point mutations for dynein IC (DIC), dic^{1} and dic^{3} (Boylan and Hays, 2002), and one deletion mutation of the dynein light chain (DLC), $robl^{k}$ (Bowman *et al.*, 1999). Western blot analysis in dynein and dynactin heterozygotes showed the expected ~50% reduction in protein levels (DHC: Figure 5, A and B; DIC: Figure S3A; DLC: Figure S3B; dynactin: Figure S4, A and B).

For dynein, *dhc* reduction resulted in an expected overall impairment of many features of retrograde transport but enhancement of a number of anterograde parameters (Figures 5, C–E, S3, C–J, and S5C, and Table S1), including significant increases in anterograde run length (Figure S3E) and average segmental velocity (Figure S3C), as well as shifts in the relative contribution of higher modes to the anterograde velocity distribution (Figures 5E and S5C and Table S1). This suggests that DHC acts as an inhibitor of anterograde transport. DLC behaved in similar manner, although the overall effect on anterograde was milder (e.g., significant increase in anterograde run length [Figure S3E], but not segmental velocity [Figure 5C]). In contrast, *dic* reduction not only led to impairment in retrograde transport but also to strong impairment in anterograde transport (Figures 5, C and D, and S3, C–J). As with kinesin, velocity modal stability was maintained in dynein reductions (Figure 5F). Thus DHC/DLC appear to act as inhibitors of anterograde movement, while DIC acts as a promoter.

In general, dynactin reduction led to bidirectional impairment of APP transport (Figures 5, G and H, and S4, C–F, and Table S1), although some variability was observed among the subunits. For *dmn* (*p50/dynamitin*), there was a mild decrease in mean retrograde segmental velocity but no significant change in anterograde velocity (Figure 5, G and H). However, there was a significant increase in both pause frequency and duration (Table S1) and in the fractions of the population of vesicles with anterograde movement (Figure S4, G–J). Perturbation of *Gl* ($p150^{Glued}$) and *grid (Arp1)* caused stronger transport impairment in terms of reduced segmental velocities and run lengths (Figures 5, G and H, and S4, C–F). However, the impairment was less pronounced in terms of increased pause frequencies and durations (Table S1). As with kinesin and dynein, velocity modes were maintained in dynactin reductions (Figure 5I). Overall, these data confirm that dynactin promotes anterograde and retrograde transport, although the transport impairment associated with perturbation in these dynactin subunits is milder than is observed for kinesin-1 and cytoplasmic dynein. In addition, these data support the notion that modal stability is a generic feature of APP transport.

Stimulation of anterograde transport by overexpression of DIC

Cytoplasmic dynein has been proposed as an activator of kinesin-1 (Martin *et al.*, 1999; Ling *et al.*, 2004; Pilling *et al.*, 2006; Kim *et al.*, 2007). Previous biochemical data established that the only detectable interactions between kinesin-1, cytoplasmic dynein, and dynactin protein complexes are mediated by DIC. Interactions were reported between DIC:$p150^{Glued}$ (Vaughan and Vallee, 1995) and DIC:KLC (Ligon *et al.*, 2004) and appear to involve similar regions of DIC (Vaughan and Vallee, 1995; Ligon *et al.*, 2004; Schroer, 2004). Previous work, however, did not distinguish whether KLC, dynactin, or both mediate the interaction between endogenous kinesin and dynein, since the in vitro work demonstrating an interaction between KLC and DIC used recombinant protein for the affinity chromatography assay (Ligon *et al.*, 2004). Thus we performed RNA interference (RNAi) experiments in S2 cells to test whether KLC binds to DIC in vivo (see *Materials and Methods*). We observed that KLC mediates binding of the KHC/KLC kinesin-1 tetramer to DIC (Figure 6A). Hence, it is possible that motor protein activity on APP vesicles is controlled by a competition between $p150^{Glued}$ and KLC for binding to DIC. Consistent with this idea, we noted that among the dynein reduction subunits, DIC reduction caused by far the strongest and most consistent impairment to bidirectional transport.

If DIC controls the balance between anterograde and retrograde transport by activating kinesin-1, overexpression of DIC would stimulate anterograde transport. To test this, we overexpressed DIC protein (see *Materials and Methods*; Figure S3K). This led to significant increases in both anterograde vesicle fraction and run length (Figure S3, E and H), as well as significant decreases in the fraction of stationary and reversing vesicles (Figure S3, G and J). In addition, the mean anterograde velocity increased significantly (Figure S3C), due to a systematic shift of each of the three velocity distribution modes toward higher center values (Figures 6D and S5D and Table S1). It should be noted that this was the only genetic condition for which we observed significant shifts in the mode centers. Taken together, these findings indicate that DIC acts as a promoter of kinesin-1 activity.

DISCUSSION

In this study, we used modest genetic alterations of kinesin-1, cytoplasmic dynein, or dynactin to probe mechanisms of axonal transport in vivo. Computer-assisted quantification of large numbers of APPYFP vesicles allowed us to achieve sufficient sensitivity for robust interpretation of the mild phenotypes induced by manipulations that maintain full organismal viability and are devoid of major uncontrolled side effects. We discovered several novel features of APP transport. First, vesicle movement driven by kinesin-1 in vivo has crucial differences from in vitro: while in vitro cargo velocity is independent of the number of motors, the velocity of kinesin-1-driven

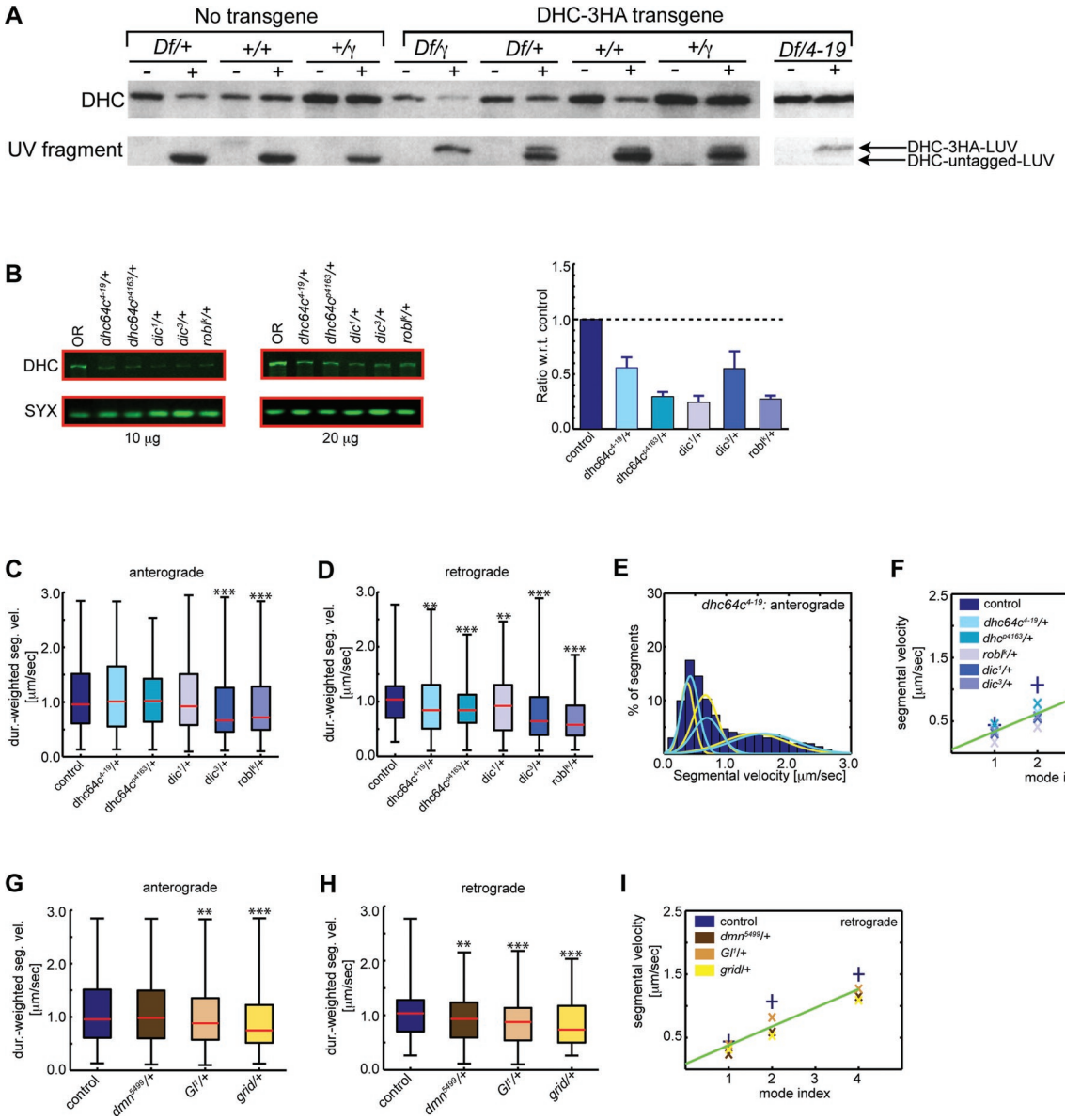

FIGURE 5: Reduction of cytoplasmic dynein and dynactin subunits confirms that modal stability is a generic feature of kinesin-1–driven APP transport. (A) Generation of *dhc* null alleles for evaluation of APP transport. Protein extracts were either treated with UV-vanadate (+) or left untreated (–) and assayed by Western blot (see *Materials and Methods*). The anti-DHC antibody recognizes endogenous DHC (the DHC-3HA transgene product) as well as the LUV fragments resulting from UV cleavage of the endogenous and transgenic DHC. Tagged and untagged LUV fragments are resolved as a doublet. Only a single LUV band (corresponding to the larger, tagged fragment) is recognized in the rescued *Df/g* genotype, consistent with the absence of endogenous DHC protein expression. Similar results are seen with the DHC allele 4-19 (far right). (B) Western blot analysis of cytoplasmic dynein reduction genotypes probed for DHC shows an ~50% reduction in $dhc64c^{4\text{-}19}$/+ and ~70% in dhc^{p4163}/+. Significant reduction in DHC is also observed in *dic* and *dlc* reduction backgrounds. (C) Reduction in *dhc* and *dlc* shows no significant effect on anterograde duration-weighted segmental velocities (mean µm/s ± SD): control, 1.09 ± 0.58; $dhc64c^{4\text{-}19}$/+, 1.14 ± 0.66; dhc^{p4163}/+, 1.06 ± 0.52; $robl^{k}$/+, 1.07 ± 0.62. Reduction in *dic* shows significant impairment in the anterograde duration-weighted segmental velocities (mean µm/s ± SD): control, 1.09 ± 0.58; dic^{1}/+, 0.91 ± 0.60; dic^{3}/+, 0.92 ± 0.55. (D) Reduction in *dhc*, *dic*, and *dlc* alleles leads to a significant decrease in retrograde duration-weighted segmental velocities (mean µm/s ± SD): control, 1.02 ± 0.41; $dhc64c^{4\text{-}19}$/+, 0.93 ± 0.50; dhc^{p4163}/+, 0.89 ± 0.38; $robl^{k}$/+, 0.93 ± 0.53; dic^{1}/+, 0.78 ± 0.48; dic^{3}/+, 0.68 ± 0.37. (E) The anterograde segmental velocity distribution of $dhc64c^{4\text{-}19}$/+ has three modes (cyan) with a shift toward occupancy of modes 2 and 3 (see Table S1; the control distribution is shown in yellow for direct comparison). Similar behavior is found for dhc^{p4163}/+. (F) Linear regression of retrograde mode centers assembled for dynein reduction genotypes shows centers that follow a ratio of ~1:2:4. (G) Reduction in Gl^{1} (p150) and *grid* (Arp1) subunits of dynactin leads to a significant decrease in mean anterograde duration-weighted segmental velocity (mean µm/s ± SD): control, 1.02 ± 0.41; dmn^{5499}/+, 1.07 ± 0.56; Gl^{1}/+, 1.00 ± 0.53; *grid*/+, 0.91 ± 0.50. (H) Reduction in *dmn* (p50/dynamitin), Gl^{1} (p150), and *grid* (Arp1) subunits of dynactin leads to a significant decrease in mean retrograde duration-weighted segmental velocity (mean µm/s ± SD): control, 1.02 ± 0.41; dmn^{5499}/+, 0.93 ± 0.44; Gl^{1}/+, 0.88 ± 0.42; *grid*/+, 0.85 ± 0.44.

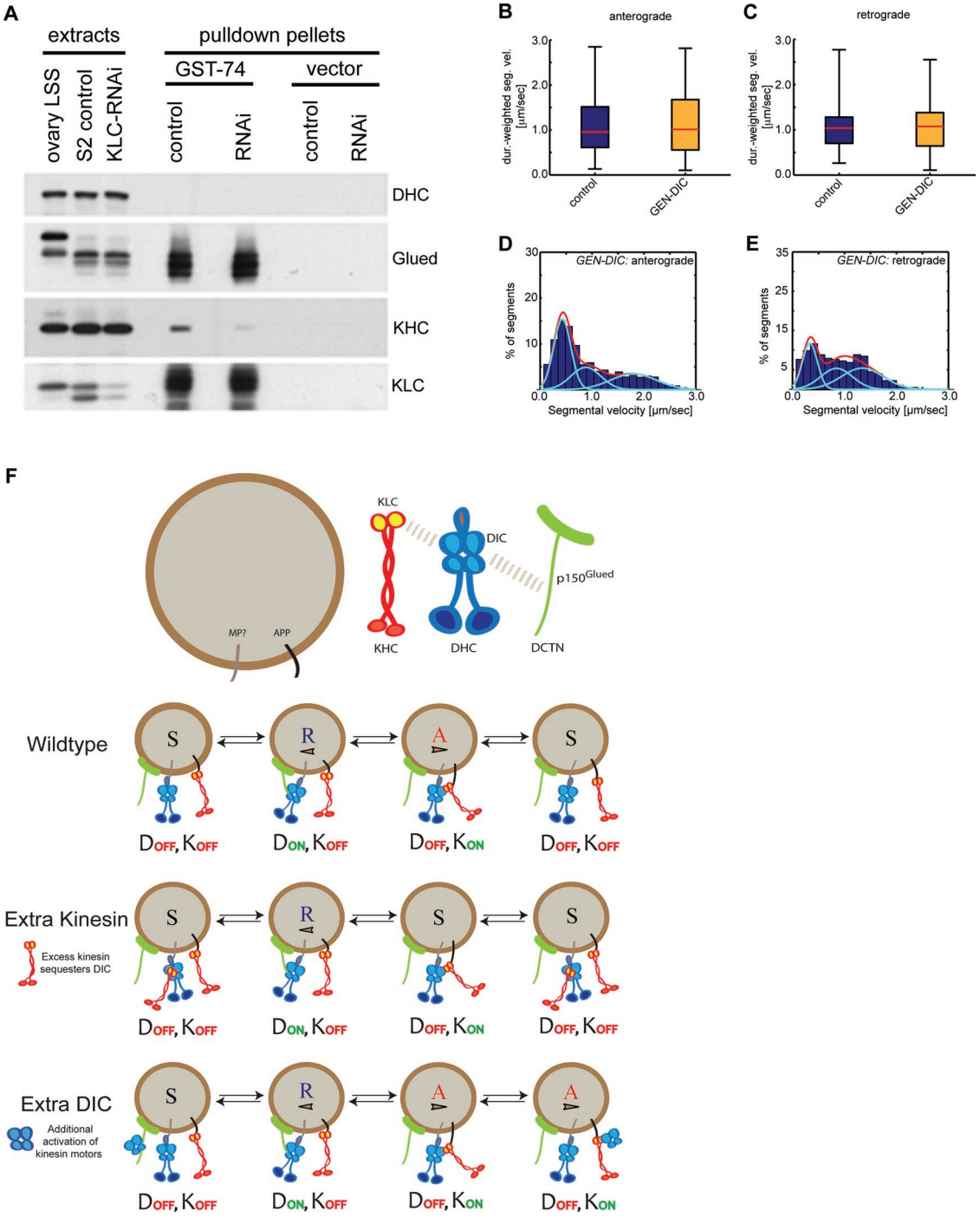

FIGURE 6: DIC stimulates anterograde APPYFP transport. (A) RNAi pulldown experiments in S2 cells demonstrate that KLC mediates binding of the KHC/KLC kinesin-1 tetramer to DIC in vivo. (B) DIC overexpression has no significant effect on mean anterograde duration-weighted segmental velocity compared with control (mean µm/s ± SD): control, 1.09 ± 0.58; GEN-DIC, 1.14 ± 0.67. However, GEN-DIC leads to a significant increase in mean anterograde unweighted segmental velocity and several other parameters of anterograde transport (Figure S3, C–J). (C) DIC overexpression has no significant effect on mean retrograde duration-weighted segmental velocity compared with control (mean µm/s ± SD): control, 1.02 ± 0.41; GEN-DIC, 1.03 ± 0.52. (D) The anterograde segmental velocity distribution of GEN-DIC has three modes (cyan) with a significant shift of mode centers toward higher values (see Table S1 and Figure S5D for a direct comparison with modes of the control distribution). Superposition of modes is shown in red. (E) The retrograde segmental velocity distribution of GEN-DIC has three modes (cyan; see Table S1 and Figure S5H for a direct comparison with modes of the control distribution). Superposition of modes is shown in red. (F) Schematic of a proposed model for APP transport under control, kinesin-1 overexpression, and DIC overexpression backgrounds (A = anterograde; R = retrograde; S = stationary). Excess kinesin-1 sequesters DIC from association with vesicle-bound KLC. This results in "decreased activation" of anterograde transport. This sequestration of DIC may also result in inhibition of retrograde transport via reduced vesicle-bound dynein or dynactin. Under excess DIC conditions, anterograde movement can be stimulated by either increased vesicle-bound DIC (i.e., cytoplasmic dynein complex) or soluble DIC associating with vesicle-bound KLC.

APP vesicles in vivo depends strongly on the number of motors. This deviates fundamentally from observations reported for lipid droplet movement (Shubeita *et al.*, 2008). Second, APP vesicles exhibit relatively stable modal velocities, suggesting the presence of stable motor assemblages on vesicles. Third, our data suggest a new and testable motor competition–coordination model of axonal transport in which direction and velocity of cargo movement are controlled at least in part by DIC.

Does the amount of kinesin-1 on APP vesicles control movement parameters?

Considerable in vitro biochemical and biophysical data indicate that kinesin-1 is highly processive. It has been proposed that the processivity originates in the strong binding of the motor head for a large fraction of the total mechanochemical cycle and the tight coordination of the binding and release of the two heads (Spudich, 1990; Howard, 2001; Gennerich and Vale, 2009). The high processivity of kinesin-1 has been postulated to be essential for long-distance vesicle movement in vivo, as it reduces the probability of cargo dissociation from microtubules.

A key prediction for processive motor transport is that the run length of cargo correlates with the number of motors bound, while the velocity is independent. Although recent work suggests that velocity of droplet movement in *Drosophila* embryos is indeed uncorrelated with the amount of active kinesin-1 (Shubeita *et al.*, 2008), multiple studies have reported kinesin-1 velocities that are too fast to easily reconcile with the in vitro rate (Howard, 2001; Kural *et al.*, 2005). This raised the possibility that both velocity and run length of kinesin-1 cargoes in vivo are dependent on the amount of available motor, a prediction fully supported by our analyses of the velocities and run lengths of kinesin-1–driven APP vesicles.

There are at least three possible explanations for this finding. First, the motor could be regulated to have a faster ATPase rate in vivo. However, this explanation does not readily account for the observation that run length and velocity of APP vesicles are correlated in vivo. Second, kinesin-1 on APP vesicles might be regulated or modified in vivo, such that the rate-limiting, strongly bound state time during the mechanochemical cycle is reduced. As a consequence, vesicle movement would show strong correlation of motor number with both run length and velocity, and run length or pause frequency would strongly depend on velocity (Spudich, 1990). Although a molecular explanation for this type of kinesin-1 behavior is lacking, recent work suggests that regions adjacent to the motor domain may control motor coordination (Crevenna *et al.*, 2008). Notably, previous work on the biophysical behavior of the coil 1 domain of KHC suggests that this structured alpha-helical coiled-coil has the unusual ability to melt at physiological temperature (de Cuevas *et al.*, 1992). Melting of this coiled-coil in vivo could reduce coordination between the heads within the kinesin-1 dimer, diminishing processivity and increasing velocity and run lengths generated by multiple kinesin-1 motors. A third possibility is that the strongly bound state time of kinesin-1 might not change in vivo, but the coiled-coil stalk domain might stretch like a spring, such that the velocity of a single kinesin-1 motor is no longer rate limiting for assembly of multiple motors on a vesicle. This possibility would also account for the observed correlation of kinesin-1 amount and run length of APP vesicles. Further biophysical work will be necessary to distinguish among these possibilities.

Our results also suggest that the assemblage of motors and their activation states on APP vesicles stay relatively constant for the majority of vesicles, even over the duration of a pause. Such "memory" on the timescale of seconds was also noted for lipid droplets (Welte *et al.*, 1998).

Movement of APP vesicles follows a multimodal velocity distribution

Although multimodal velocity distributions of active cargo transport have been identified previously in vitro and in vivo (Hill *et al.*, 2004; Levi *et al.*, 2006; Gagliano *et al.*, 2010), we made several new findings in this study. First, we analyzed and inferred multimodal velocity distributions using different computational and statistical analysis methods and assumptions. Previous studies (Hill *et al.*, 2004; Levi *et al.*, 2006; Gagliano *et al.*, 2010) assumed a model in which multiple motors share their mechanical load. Consequently, it was assumed that higher-velocity modes are multiples of the lowest mode, presumably generated by a single motor, and that each velocity mode has the same spread (i.e., variance). We made no such assumptions in our analysis. Instead, we reason that multiple factors may be involved in determining velocities of actively transported cargoes and thus prefer an approach that permits varying spread within each mode and varying separation between neighboring modes. Our analysis consistently identified three velocity modes that follow a ratio of ~1:2:4 in both anterograde and retrograde directions. The identified velocity modes we identified are not equally spaced and have different variances, with higher velocity modes associated with larger variances. Second, we identified how different genetic manipulations of individual units of the molecular motor machinery may differentially shift relative contributions of individual modes. Our analysis consistently returned three velocity modes that follow a ratio of 1:2:4 in all genetic backgrounds we analyzed. This provides further support for the analysis method we used. Third, we found that velocities of individual APP vesicles are relatively stable based on computational analysis of transition probabilities between different modes. Such analysis provides new insights into the dynamic behavior of individual cargoes.

The in vivo behavior of APP vesicles is inconsistent with most current models for control of vesicle movement

In agreement with previous work on lipid droplets, melanosomes, and other nonneuronal cargoes, our data do not support simple tug-of-war or exclusionary presence models and are most consistent with coordination models (Gross, 2004; Kural *et al.*, 2005). For example, an exclusionary presence model for APP axonal vesicles predicts that reduction of kinesin-1 motors should have either no effect or increased retrograde transport, while reduction of dynein motors should have no effect or increased anterograde transport. Similarly, increased kinesin-1 is predicted to have either no effect or increased anterograde transport and decreased retrograde transport. For simple tug-of-war models, the prediction is that simultaneous attachment and activity of opposing motors would generate net APP movement in one direction or another, depending on the relative number of each type of motor attached to a vesicle (Muller *et al.*, 2008; Soppina *et al.*, 2009). Thus reduction of either kinesin-1 or cytoplasmic dynein would be predicted to uniformly stimulate movement in the opposite direction, which is inconsistent with many of our observations. A more sophisticated tug-of-war model (Ally *et al.*, 2009) proposed that dynein activity is needed to activate kinesin-1 and vice versa. Indeed, in agreement with previous reports, kinesin reductions seemed to inhibit dynein-driven movements (Brady *et al.*, 1990; Martin *et al.*, 1999; Pilling *et al.*, 2006; Kim *et al.*, 2007; Colin *et al.*, 2008). However, although we cannot completely exclude direct effects of kinesin-1 reduction on cytoplasmic dynein activity, sampling bias is a compelling explanation for the impaired

dynein-driven retrograde transport upon kinesin-1 reduction (see Figure 4, F–H). More importantly, our finding that reductions in DHC enhance anterograde movement is inconsistent with the model proposed by Ally and coworkers (Ally *et al.*, 2009).

A computational model of motor-driven transport was recently proposed (Muller *et al.*, 2008) in which multiple kinesin and dynein motors interact indirectly via their nonlinear, force-dependent unbinding rates. This yields a nonintuitive coordination mechanism whereby vesicle movement in a specific direction is driven predominantly by one type of motor. We tested several predictions of this model using our data. First, when the plus end–directed and minus end–directed motors are asymmetric, the model predicts that anterograde and retrograde vesicle movement each follow a single peak-velocity distribution. However, our APPYFP data reveal that distributions of both anterograde and retrograde velocities are much wider and exhibit multiple modes. Second, the model proposes that weak motors with a small ratio of stall-to-detachment forces drives stationary cargoes classified under the category of "no motion." Consequently, the model predicts that a significant increase in the fraction of stationary cargoes results from increases in both weak plus end–directed and minus end–directed motors. In fact, significant increases in the fraction of stationary cargoes are observed in many of our reduction genotypes. For example, KHC reductions (khc^{8}/+ and khc^{20}/+) cause a twofold increase in the fraction of stationary cargoes (Figure S2E). This would require a concurrent increase in the fraction of "weak" dynein motors, which seems at odds with the basic model assumption that changes to kinesin do not alter the inherent properties of dynein motors and vice versa. Finally, although changing the parameters of the motors can account for changes to stall force, run length, pause time, and velocity caused by different dynein mutations in the lipid droplet system, this model cannot account for the changes we observe for APP vesicles in the population distribution of different types of cargoes (anterograde, retrograde, stationary, and reversing). For example, the model cannot explain why there is a substantial fraction (~40%) of stationary APPYFP vesicles in the control group and why there are different fractions of anterograde (~32%) and retrograde (18%) cargoes. These arguments suggest that mechanical coordination alone cannot fully account for the behavior of APP axonal transport.

A competition–coordination mechanism regulates axonal transport of APP vesicles

In a typical coordination model, vesicles bind to both kinesin-1 and cytoplasmic dynein simultaneously, and a coordination process on the vesicle surface ensures that both types of motors are not active at the same time (Gross, 2004). The predictions of this model are ambiguous, given the lack of a defined coordination mechanism. However, if kinesin and dynein themselves are part of the coordination mechanism, this model would predict that reductions of either kinesin-1 or cytoplasmic dynein might impair movement in both directions. For vesicle transport in the lipid droplet system, it was argued that a coordination model best accounts for the experimental observations. Our data constrain the type of coordination model that can be proposed. We find that: 1) reducing kinesin-1 does not decrease cytoplasmic dynein levels on floated vesicles, and hence kinesin-1 is not required for cytoplasmic dynein association with vesicles; 2) overexpression of kinesin-1 does not stimulate dynein-driven retrograde transport, suggesting that kinesin-1 binding to DIC does not stimulate dynein activity; 3) sampling effects in kinesin-1 reduction may account for decreases in retrograde movement; and 4) modest overexpression of DIC leads to a significant increase in retrograde run length but a much greater stimulatory effect is observed for anterograde movement in terms of distribution and occupancy of velocity modes toward faster-moving modes, longer anterograde run lengths, and a large increase in the ratio of anterograde to retrograde movement (a shift from 1.8:1 to 2.3:1). Thus a formal genetic interpretation of our results implicates DIC as an activator of kinesin-1–mediated anterograde transport. Combining these genetic findings with biochemical evidence for the ability of DIC to bind $p150^{Glued}$ and KLC in similar regions (Ligon *et al.*, 2004) leads to a simple model in which the activity of kinesin-1 and cytoplasmic dynein is coordinated by competition of dynactin and kinesin-1 for binding to DIC, thereby controlling the direction of movement (Figure 6F). This model proposes that the binding of dynactin to DIC promotes retrograde transport and binding of DIC to KLC promotes anterograde transport. Excess soluble kinesin-1 is predicted to compete with vesicle-bound dynactin for DIC binding, resulting in impaired activation of cytoplasmic dynein. Similarly, excess kinesin-1 is predicted to compete with vesicle-bound KLC for DIC binding, causing impaired kinesin-1 movement. Indeed, our data exhibit reduced bidirectional transport in kinesin-1 overexpression (Figures 4, D and E, and S2, A–D and I–L). On the other hand, the model predicts that excess soluble DIC binds preferentially to KLC on APP vesicles, resulting in enhanced anterograde transport bias. Indeed, for vesicles in the GEN (genomic)-DIC genotype, we found a marked increase in anterograde population percentage, faster average segmental velocities, increase in occupancy and mean value of mode 3 (fastest mode), and extended anterograde run lengths (Figure S3, G, C, D, and E, respectively, and Table S1). Thus DIC activates anterograde transport and biases axonal transport in the anterograde direction. The precise mechanism for this bias in GEN-DIC is an interesting question warranting further investigation. Intriguingly, we also observed that overexpression of DIC increased bidirectional pause frequency and duration (Table S1). Because this occurred in both anterograde and retrograde directions and without reduction in duration-weighted segmental velocities (Figure 6, B and C), it is possible that increased density of non-APP vesicles (obstacles) along the axon indirectly interferes and/or temporarily stalls vesicle movement in this genotype. Taken together, our data provide strong quantitative support for a competition–coordination mechanism for the in vivo axonal transport of APP in which DIC–KLC interactions define a switch in the control of retrograde and anterograde movement. Previous overexpression studies in nonneuronal cells were interpreted to mean that excess DIC poisons retrograde transport (King *et al.*, 2003). However, unlike our live-cell measurements, previous fixed-cell analyses could not distinguish inhibition of retrograde transport from stimulation of anterograde transport or a combination of the two. Still, we cannot completely exclude that some aspects of our data might represent indirect effects of protein overexpression on transport (i.e., due to aberrant transport/sequestration of known or unknown regulators of motor proteins). For example, kinesin-1 overexpression did not yield faster anterograde velocities, indicating that additional regulatory factors are required (Gindhart *et al.*, 2003; Blasius *et al.*, 2007). Further investigations will be needed to test the many detailed predictions of our model. In addition, a search for various proteins interacting with $p150^{Glued}$, DIC, and KLC may augment our understanding of how the interactions between DIC, dynactin, and/or KLC may be modulated.

Finally, the rich biological diversity observed within and across microtubule motor families, coupled to the unique protein constitution of different cargo types, as well as multiple regulators of axonal transport, raises the possibility that no single universal mechanism may emerge for axonal transport. Indeed, controversies in the literature

may reflect this heterogeneity. These differences highlight the importance of employing well-characterized vesicles in the study of axonal transport in vivo. Our ability to rescue axonal transport defects seen in a variety of neurodegenerative diseases affecting humans will likely require thorough understanding of the molecular mechanisms governing the transport of specific cargo types. Given the association of APP and Alzheimer's disease, we hope our study sets the stage for focused probing and greater insight into mechanisms of neurodegeneration and therapeutic targets in this field.

MATERIALS AND METHODS

Genetics

Drosophila stocks were maintained at room temperature or at 25°C, except when crosses were set up at 29°C for imaging of L3 larvae. UAS-APPYFP (X) controls carry the human APP695 transgene tagged with YFP and inserted in the X chromosome. Only female L3 larvae were used for imaging. In brief, L3 larvae expressing UAS-APPYFP arose from crosses between UAS-APPYFP males and SG26.1Gal4 females. Male animals did not express UAS-APPYFP and thus provided an internal control. Motor gene reductions were obtained by first generating a UAS-APPYFP; pin^{88K}/B3 stable stock (the B3 chromosome carries T(2:3) CyO, TM6B with the dominant markers Hu, Tb, and Cyo).

For kinesin-1 reduction studies, three alleles were used: khc^{8}/CyO, khc^{20}/CyO, and klc^{8ex94}/TM6B. The *khc* alleles are null point mutants whose translated fragments are thought to be degraded due to instability (Saxton *et al.*, 1991; Hurd and Saxton, 1996; Hurd *et al.*, 1996; Brendza *et al.*, 2000). The *klc* allele is a deletion allele spanning the entire *klc* gene in chromosome 3 (Gindhart *et al.*, 1998). UAS-APPYFP; pin^{88K}/B3 females were crossed to khc^{8}/CyO, khc^{20}/CyO, or klc^{8ex94}/TM6B males. Selected UAS-APPYFP/Y; *kinesin*/B3 males were then crossed to SG26.1Gal4 females. Non-tubby L3 females were selected for imaging.

For cytoplasmic dynein reduction studies, five alleles were used: $dhc64c^{p4163}$/TM6B, $dhc64c^{4-19}$/TM6B, dic^{1}/FM7GFP, dic^{3}/FM7GFP, and $robl^{k}$/CyO. The $dhc64c^{p4163}$ allele has an internal 122–base pair deletion of nucleotides 5750–5871 (with respect to the Dhc64C cDNA), which is predicted to remove P-loop 1 and lead to premature termination of translation upstream of P-loops 2–4. Western blot analysis of these mutations confirms that $dhc64c^{4-19}$ and $dhc64c^{p4163}$ are null or near-null alleles (Figure 5A). The *dic* alleles have been characterized as loss of function, with dic^{1} being functionally stronger than dic^{3} (Boylan and Hays, 2002). The *dlc* allele $robl^{k}$ is a deletion allele spanning the entire *robl* gene (Bowman *et al.*, 1999). For crosses involving *dhc* or *dlc*, we followed the procedure used for kinesin-1. For *dic* crosses, UAS-APPYFP/Y; SG26.1Gal4/B3 animals were crossed to dic^{1}/FM7GFP or dic^{3}/FM7GFP, and a fluorescence microscope was used to select female L3 larvae negative for GFP—these animals are UAS-APPYFP/*dic*; SG26.1Gal4/+.

For dynactin reduction studies, three alleles were used: *grid*/TM6B, dmn^{5499}/CyO, and Gl^{1}/In(3L)D, d^{1} (BL-2394). The *grid* allele has been characterized as a loss-of-function point mutant (Haghnia *et al.*, 2007). The dmn^{5499} allele, kindly provided by Jason Duncan (Willamette University, Salem, OR), is also thought to be a loss-of-function point mutant (unpublished observations). The Gl^{1} allele is thought to be dominant negative. As with kinesin-1, UAS-APPYFP; pin^{88K}/B3 virgins were crossed to *grid*/TM6B, dmn^{5499}/CyO, or Gl^{1}/In(3L)D, d^{1} (BL-2394 Bloomington stock). Selected UAS-APPYFP/Y; *dynactin*/B3 males were then crossed to SG26.1Gal4 females, and non-tubby L3 females were selected for imaging.

For kinesin-1 overexpression experiments, we used GEN-KLC/CyO; TM3/TM6B and *sp*/CyO; GEN-KHC stocks (Saxton *et al.*, 1991; Gindhart *et al.*, 1998). To achieve overexpression of both kinesin-1 subunits, we crossed GEN-KLC; GEN-KHC females to UAS-APPYFP/Y; SG26.1Gal4/B3 males. UAS-APPYFP/X; GEN-KLC/+; GEN-KHC/SG26.1 animals were used for imaging.

For cytoplasmic dynein overexpression experiments, we used a GEN-DIC stock (Boylan and Hays, 2002). In brief, UAS-APPYFP/Y; GEN-DIC/B3 males were generated and crossed to SG26.1 virgins. UAS-APPYFP/X; GEN-DIC/+; SG26.1/+ L3 larvae were then selected for imaging.

Microscopy

L3 larvae were dissected and imaged on a 3 cm^2 Sylgard platform using Ca^{2+}-free medium consisting of NaCl (128 mM), ethylene glycol tetraacetic acid (EGTA; 1 mM), MgCl2 (4 mM), KCl (2 mM), HEPES (5 mM), and sucrose (36 mM). Dissected animals were inverted onto a coverslip and imaged using a Nikon Eclipse TE2000-U inverted microscope with a CoolSNAP HQ camera (Roper Scientific, Surrey, BC, Canada) and a 100×/1.40 numerical aperture (NA) oil objective. Images were collected at 10 frames/s with 100 ms exposure for 15 s under the control of MetaMorph software (MDS Analytical Technologies, Sunnyvale, CA). For each genotype, four time-lapse movies were collected for each animal (10 animals were imaged for analysis).

Western blot analysis

To characterize *Dhc64C* gene mutations, we crossed balanced females carrying the γ4163a or *4-19* mutations to males expressing the DHC-3HA transgene and a deficiency (*Df*) that removes the *Dhc64C* gene. Progeny of genotype *Df/γ* or *Df/4-19* survive only in the presence of the transgene. Protein extracts from all the female progeny classes were either treated with UV-vanadate (+) or left untreated (–) and then assayed by Western blot. The blot was probed with an anti-DHC antibody that recognizes endogenous DHC (the DHC-3HA [hemagglutinin] transgene product) and the LUV (light ultraviolet cleavage fragment) fragments resulting from UV cleavage of the endogenous and transgenic DHC. Tagged and untagged LUV fragments are resolved as a doublet. Only a single LUV band is recognized in rescued *Df/γ* or *Df/4-19* flies, corresponding to the higher-molecular-weight tagged fragment. This is consistent with the absence of endogenous DHC protein expression.

Protein analysis of kinesin-1, cytoplasmic dynein, and dynactin genetic reduction and overexpression backgrounds was performed using Western blot and quantified with an Odyssey system (LI-COR Biosciences, Lincoln, NE). In brief, 10 animals were homogenized in 100 µl 2X LDS sample buffer (Invitrogen, Carlsbad, CA) with 2% β-mercaptoethanol. Samples were heated for 10 min at 98°C and centrifuged for 5 min at 14,000 rpm. The supernatant was then removed, and protein concentration was measured using the Bio-Rad DC protein assay (Hercules, CA). Samples were loaded on precast 4–12% Bis-Tris gels (Invitrogen), and See-Plus 2 (Invitrogen) was used as the molecular-weight marker. Transfer to nitrocellulose membranes was done at 4°C using a wet system and buffer consisting of 25 mM Tris base, 190 mM glycine, and 20% methanol. Membranes were incubated in primary antibody overnight at 4°C. Incubation in secondary antibody (1:5000; Odyssey) was 2 h at room temperature. Quantification was done using Odyssey software (Li-Cor, Lincoln, NE)

Antibodies

Anti-KHC (Cytoskeleton, Denver, CO), anti-KLC (Goldstein lab), anti-DHC (P1H4; McGrail and Hays, 1997), anti-DIC (Chemicon International, Temecula, CA), anti-ROBL (Bowman *et al.*, 1999), anti-Arp1

(Haghnia *et al.*, 2007), anti-p50 (Duncan and Warrior, 2002), and anti-syntaxin (8C3; Developmental Studies Hybridoma Bank, University of Iowa, Iowa City, IA) were used as described or as recommended by the manufacturer. Many commercially available anti-p150 antibodies were tested, but none recognized *Drosophila* p150. Additionally, RNAi pulldown experiments utilized polyclonal anti-glued antibody (Waterman-Storer and Holzbaur, 1996) and a polyclonal *pan*-anti-KLC antibody (Khodjakov *et al.*, 1998).

Membrane flotation assay

After raising *yw* and khc^{8}/+ animals at 25°C, we collected ~7.5 ml of adult flies in a 50-ml conical tube and immediately snap-froze them in liquid nitrogen. The tubes were shaken to separate heads from bodies, and fly heads were collected using a sieving system (Slemmon *et al.*, 1982). Heads were then homogenized in 0.75 ml homogenization buffer composed of 8% sucrose plus 1 mM imidazole. Debris was removed by centrifugation at 1500 × *g* for 10 min at 4°C, and the PNS was collected. The pellet was then resuspended in 0.75 ml homogenization buffer and centrifuged for 5 min at 1500 × *g*. The supernatant was collected and combined with the PNS, which was centrifuged at 10,000 × *g* for 5 min to remove mitochondria. The resulting supernatant was carefully removed so as not to disturb the pellet and was mixed with 62% sucrose to a final concentration of 40% sucrose ("input"). The input was bottom-loaded in an 11 × 34 mm Beckman polycarbonate tube and overlaid with two 0.7 ml cushions of 35 and 8% sucrose. Tubes were spun at 200,000 × *g* for 2 h at 4°C. The 8/35% interface, which contains light membrane-bound organelles and associated proteins (Haghnia *et al.*, 2007) was collected and assayed by SDS–PAGE and Western blotting.

KLC-RNAi pulldown assay

KLC RNAi expression in S2 cells was achieved by a double-stranded RNA preparation with a Megascript T7 kit (Applied Biosystems, Bedford, MA) and the following primers: *sense* 5′-t7-CTCGAAGCCTTGCGAGTGG-3′ and *antisense* 5′-t7-AGAGTACGGAGACGCGCTG-3′. An N-terminal glutathione *S*-transferase (GST)-fusion protein of full-length *Drosophila* DIC ("GST-74") was expressed in *Escherichia coli* and bound to glutathione Sepharose 4B beads (GE Healthcare, Waukesha, WI). Control S2 cells and RNAi-treated cells were homogenized in PMEG buffer (100 mM PIPES, 5 mM MgOAc, 5 mM EGTA, 0.5 mM EDTA, 0.9 M glycerol, 1 mM dithiothreitol; pH 6.9) with protease inhibitors. TX-100 0.1% was added, and the cells were centrifuged at 12,000 × *g* for 10 min at 4°C. Supernatants were precleared against washed beads and subsequently incubated with GST-74 beads (or control beads bound to GST alone) for 2 h at 4°C. Beads were washed three times, and bound proteins were eluted into SDS–PAGE sample buffer for analysis by Western blot using 6–10% gradient gel and 15 μg protein.

Single-particle tracking and computational analysis of APPYFP vesicle movement

APPYFP vesicles in time-lapse movies were detected as particles (Ponti *et al.*, 2003; see Supplemental Movie S2). Their full trajectories were recovered using customized software based on a modification of the single-particle tracking technique described previously (Yang *et al.*, 2005). For vesicles crossing one another during bidirectional transport, trajectories were first resolved using a global bipartite linear assignment algorithm that minimizes total variations of intensity, velocity, and direction of movement for each vesicle. The output of this step contains mostly trajectory segments, so an additional process was performed to link these segments into full trajectories using a multiple hypothesis-testing algorithm (Blackman, 1999). A manual process was subsequently used to recover trajectories the software was unable to recover. Finally, all recovered trajectories were individually inspected, and errors were corrected. This process is able to recover more than 95% of all vesicle trajectories that fully reside in the microscope field of view.

For each genotype, individual cargoes were classified as being stationary, anterograde, retrograde, or reversing. Cargo trajectories of each genotype were then analyzed by calculating overall distribution of cargo population, as well as individual cargo velocity, run length, pause, and reversal (see Supplemental Material). Data analysis was conducted using customized software written in MATLAB (MathWorks, Natick, MA) and C++. Segmental velocities were defined as the mean velocity of a trajectory segment uninterrupted by a pause, reversal, or movie termination event. Duration-weighted segmental velocity evaluates the average velocity behavior that vesicles exhibit per time spent moving. Unweighted segmental velocity reports the average velocity without considering the duration of different trajectory segments. Estimated run length was calculated by dividing the mean segmental velocity by the total pause frequency.

Statistical analysis

Data were first checked for normality using three different tests in the *nortest* package of *R*: the Lilliefors test, the Anderson-Darling test, and the Shapiro-Francis test. For those that followed normal distributions, their means and distributions were compared using pairwise two-sample, two-sided Student's *t* tests and Kolmogorov-Smirnov tests, respectively. For nonnormal distributions, nonparametric tests, including permutation tests (Moore and McCabe, 2005) and Wilcoxon tests, were used (see Supplemental Material).

Modes in cargo velocities were identified by model-based clustering of the collection of all cargo segmental velocities using the *mclust* package of *R* (Fraley and Raftery, 2002). For each individual cargo, the mode of its segmental velocities can be determined using standard pattern classification techniques (Theodoridis and Koutroumbas, 2009). Specifically, we compared the segmental velocity modes of each individual cargo in three cases: 1) before and after a pause; 2) before and after a reversal; and 3) on initiation and termination of a track segment. By repeating this analysis for all individual cargoes, we calculated the ensemble probabilities of transition between modes (i.e., probabilities of cargoes remaining in the same segmental velocity mode and switching between different modes). To examine whether individual cargoes stably maintain their velocity modes, we calculated the theoretical mode transition probabilities if cargoes were to randomly switch between different velocity modes (see Supplemental Material).

ACKNOWLEDGMENTS

This work was supported in part by grants from the National Institutes of Health to G.R. (Ruth L. Kirschstein NRSA-5F31AG024672), G.D. (U01-GM067230), and L.S.B.G. (GM35252 and AG032180) and by a Burroughs-Wellcome LJIS Fellowship to G.Y. We thank Angels Almenar, Kristi Bache, Jason Duncan, Tomas Falzone, Kristina Schimmelpfeng, and other members of the Goldstein lab for reagents and intellectual input. We thank Madeline Serr for work on the RNA pulldown assay. L.S.B.G. is a Howard Hughes Medical Institute investigator. The 8C3 anti-syntaxin antibody was obtained from the Developmental Studies Hybridoma Bank developed under the auspices of the National Institute of Child Health and Human Development and maintained by the University of Iowa Department of Biology, Iowa City, IA.

REFERENCES

Ally S, Larson AG, Barlan K, Rice SE, Gelfand VI (2009). Opposite-polarity motors activate one another to trigger cargo transport in live cells. J Cell Biol 187, 1071–1082.

Amaratunga A, Leeman SE, Kosik KS, Fine RE (1995). Inhibition of kinesin synthesis in vivo inhibits the rapid transport of representative proteins for three transport vesicle classes into the axon. J Neurochem 64, 2374–2376.

Amaratunga A, Morin PJ, Kosik KS, Fine RE (1993). Inhibition of kinesin synthesis and rapid anterograde axonal transport in vivo by an antisense oligonucleotide. J Biol Chem 268, 17427–17430.

Blackman S (1999). Design and Analysis of Modern Tracking Systems, Norwood, MA: Artech House.

Blasius TL, Cai D, Jih GT, Toret CP, Verhey KJ (2007). Two binding partners cooperate to activate the molecular motor Kinesin-1. J Cell Biol 176, 11–17.

Block SM, Goldstein LS, Schnapp BJ (1990). Bead movement by single kinesin molecules studied with optical tweezers. Nature 348, 348–352.

Bowman AB, Patel-King RS, Benashski SE, McCaffery JM, Goldstein LS, King SM (1999). *Drosophila* roadblock and *Chlamydomonas* LC7: a conserved family of dynein-associated proteins involved in axonal transport, flagellar motility, and mitosis. J Cell Biol 146, 165–180.

Boylan KLM, Hays TS (2002). The gene for the intermediate chain subunit of cytoplasmic dynein is essential in *Drosophila*. Genetics 162, 1211–1220.

Brady ST, Pfister KK, Bloom GS (1990). A monoclonal antibody against kinesin inhibits both anterograde and retrograde fast axonal transport in squid axoplasm. Proc Natl Acad Sci USA 87, 1061–1065.

Brendza RP, Sheehan KB, Turner FR, Saxton WM (2000). Clonal tests of conventional kinesin function during cell proliferation and differentiation. Mol Biol Cell 11, 1329–1343.

Chevalier-Larsen E, Holzbaur EL (2006). Axonal transport and neurodegenerative disease. Biochim Biophys Acta 1762, 1094–1108.

Colin E, Zala D, Liot G, Rangone H, Borrell-Pages M, Li XJ, Saudou F, Humbert S (2008). Huntingtin phosphorylation acts as a molecular switch for anterograde/retrograde transport in neurons. EMBO J 27, 2124–2134.

Crevenna AH, Madathil S, Cohen DN, Wagenbach M, Fahmy K, Howard J (2008). Secondary structure and compliance of a predicted flexible domain in kinesin-1 necessary for cooperation of motors. Biophys J 95, 5216–5227.

de Cuevas M, Tao T, Goldstein LS (1992). Evidence that the stalk of *Drosophila* kinesin heavy chain is an alpha-helical coiled coil. J Cell Biol 116, 957–965.

De Vos KJ, Grierson AJ, Ackerley S, Miller CCJ (2008). Role of axonal transport in neurodegenerative diseases. Annu Rev Neurosci 31, 151–173.

Duncan JE, Goldstein LS (2006). The genetics of axonal transport and axonal transport disorders. PLoS Genet 2, e124.

Duncan JE, Warrior R (2002). The cytoplasmic dynein and kinesin motors have interdependent roles in patterning the *Drosophila* oocyte. Curr Biol 12, 1982–1991.

Ferreira A, Niclas J, Vale R, Banker G, Kosik K (1992). Suppression of kinesin expression in cultured hippocampal neurons using antisense oligonucleotides. J Cell Biol 117, 595–606.

Fraley C, Raftery AE (2002). Model-based clustering, discriminant analysis and density estimation. J Am Stat Assoc 97, 611–631.

Gagliano J, Walb M, Blaker B, Macosko JC, Holzwarth G (2010). Kinesin velocity increases with the number of motors pulling against viscoelastic drag. Eur Biophys J 39, 801–813.

Gennerich A, Carter AP, Reck-Peterson SL, Vale RD (2007). Force-induced bidirectional stepping of cytoplasmic dynein. Cell 131, 952–965.

Gennerich A, Vale RD (2009). Walking the walk: how kinesin and dynein coordinate their steps. Curr Opin Cell Biol 21, 59–67.

Gindhart JG, Chen J, Faulkner M, Gandhi R, Doerner K, Wisniewski T, Nandlestadt A (2003). The kinesin-associated protein UNC-76 is required for axonal transport in the *Drosophila* nervous system. Mol Biol Cell 14, 3356–3365.

Gindhart JG, Jr., Desai CJ, Beushausen S, Zinn K, Goldstein LS (1998). Kinesin light chains are essential for axonal transport in *Drosophila*. J Cell Biol 141, 443–454.

Goldsbury C, Mocanu MM, Thies E, Kaether C, Haass C, Keller P, Biernat J, Mandelkow E, Mandelkow EM (2006). Inhibition of APP trafficking by tau protein does not increase the generation of amyloid-β peptides. Traffic 7, 873–888.

Goldstein LS (2003). Do disorders of movement cause movement disorders and dementia? Neuron 40, 415–425.

Goldstein LS, Yang Z (2000). Microtubule-based transport systems in neurons: the roles of kinesins and dyneins. Annu Rev Neurosci 23, 39–71.

Grafstein B, Forman DS (1980). Intracellular transport in neurons. Physiol Rev 60, 1167–1283.

Gross SP (2004). Hither and yon: a review of bi-directional microtubule-based transport. Phys Biol 1, R1–R11.

Gross SP, Welte MA, Block SM, Wieschaus EF (2002). Coordination of opposite-polarity microtubule motors. J Cell Biol 156, 715–724.

Gunawardena S, Goldstein LS (2001). Disruption of axonal transport and neuronal viability by amyloid precursor protein mutations in *Drosophila*. Neuron 32, 389–401.

Haghnia M, Cavalli V, Shah SB, Schimmelpfeng K, Brusch R, Yang G, Herrera C, Pilling A, Goldstein LS (2007). Dynactin is required for coordinated bidirectional motility, but not for dynein membrane attachment. Mol Biol Cell 18, 2081–2089.

Hill DB, Plaza MJ, Bonin K, Holzwarth G (2004). Fast vesicle transport in PC12 neurites: velocities and forces. Eur Biophys J 33, 623–632.

Hirokawa N, Takemura R (2005). Molecular motors and mechanisms of directional transport in neurons. Nat Rev Neurosci 6, 201–214.

Howard J (2001). Mechanics of Motor Proteins and the Cytoskeleton, Sunderland, MA: Sinauer Associates.

Howard J, Hudspeth AJ, Vale RD (1989). Movement of microtubules by single kinesin molecules. Nature 342, 154–158.

Hurd DD, Saxton WM (1996). Kinesin mutations cause motor neuron disease phenotypes by disrupting fast axonal transport in *Drosophila*. Genetics 144, 1075–1085.

Hurd DD, Stern M, Saxton WM (1996). Mutation of the axonal transport motor kinesin enhances paralytic and suppresses Shaker in *Drosophila*. Genetics 142, 195–204.

Inomata H, Nakamura Y, Hayakawa A, Takata H, Suzuki T, Miyazawa K, Kitamura N (2003). A scaffold protein JIP-1b enhances amyloid precursor protein phosphorylation by JNK and its association with kinesin light chain 1. J Biol Chem 278, 22946–22955.

Kaether C, Skehel P, Dotti CG (2000). Axonal membrane proteins are transported in distinct carriers: a two-color video microscopy study in cultured hippocampal neurons. Mol Biol Cell 11, 1213–1224.

Kamal A, Almenar-Queralt A, LeBlanc JF, Roberts EA, Goldstein LS (2001). Kinesin-mediated axonal transport of a membrane compartment containing β-secretase and presenilin-1 requires APP. Nature 414, 643–648.

Kamal A, Stokin GB, Yang Z, Xia CH, Goldstein LS (2000). Axonal transport of amyloid precursor protein is mediated by direct binding to the kinesin light chain subunit of kinesin-I. Neuron 28, 449–459.

Karki S, Holzbaur EL (1999). Cytoplasmic dynein and dynactin in cell division and intracellular transport. Curr Opin Cell Biol 11, 45–53.

Khodjakov A, Lizunova EM, Minin AA, Koonce MP, Gyoeva FK (1998). A specific light chain of kinesin associates with mitochondria in cultured cells. Mol Biol Cell 9, 333–343.

Kim H, Ling SC, Rogers GC, Kural C, Selvin PR, Rogers SL, Gelfand VI (2007). Microtubule binding by dynactin is required for microtubule organization but not cargo transport. J Cell Biol 176, 641–651.

King SJ, Brown CL, Maier KC, Quintyne NJ, Schroer TA (2003). Analysis of the dynein-dynactin interaction in vitro and in vivo. Mol Biol Cell 14, 5089–5097.

King SJ, Schroer TA (2000). Dynactin increases the processivity of the cytoplasmic dynein motor. Nat Cell Biol 2, 20–24.

King SM (2000). The dynein microtubule motor. Biochim Biophys Acta 1496, 60–75.

Koo EH, Sisodia SS, Archer DR, Martin LJ, Weidemann A, Beyreuther K, Fischer P, Masters CL, Price DL (1990). Precursor of amyloid protein in Alzheimer disease undergoes fast anterograde axonal transport. Proc Natl Acad Sci USA 87, 1561–1565.

Kural C, Kim H, Syed S, Goshima G, Gelfand VI, Selvin PR (2005). Kinesin and dynein move a peroxisome in vivo: a tug-of-war or coordinated movement. Science 308, 1469–1472.

Kwinter DM, Lo K, Mafi P, Silverman MA (2009). Dynactin regulates bidirectional transport of dense-core vesicles in the axon and dendrites of cultured hippocampal neurons. Neuroscience 162, 1001–1010.

Lawrence CJ *et al.* (2004). A standardized kinesin nomenclature. J Cell Biol 167, 19–22.

Levi V, Serpinskaya AS, Gratton E, Gelfand V (2006). Organelle transport along microtubules in *Xenopus* melanophores: evidence for cooperation between multiple motors. Biophys J 90, 318–327.

Ligon LA, Tokito M, Finklestein JM, Grossman FE, Holzbaur EL (2004). A direct interaction between cytoplasmic dynein and kinesin I may coordinate motor activity. J Biol Chem 279, 19201–19208.

Ling SC, Fahrner PS, Greenough WT, Gelfand VI (2004). Transport of *Drosophila* fragile X mental retardation protein-containing ribonucleoprotein granules by kinesin-1 and cytoplasmic dynein. Proc Natl Acad Sci USA 101, 17428–17433.

Martin M, Iyadurai SJ, Gassman A, Gindhart JG, Jr., Hays TS, Saxton WM (1999). Cytoplasmic dynein, the dynactin complex, and kinesin are interdependent and essential for fast axonal transport. Mol Biol Cell 10, 3717–3728.

Matsuda S, Matsuda Y, D'Adamio L (2003). Amyloid beta protein precursor (AbetaPP), but not AbetaPP-like protein 2, is bridged to the kinesin light chain by the scaffold protein JNK-interacting protein 1. J Biol Chem 278, 38601–38606.

McGrail M, Hays TS (1997). The microtubule motor cytoplasmic dynein is required for spindle orientation during germline cell divisions and oocyte differentiation in *Drosophila*. Development 124, 2409–2419.

Moore DS, McCabe GP (2005). Introduction to the Practice of Statistics, 5th ed., New York: W. H. Freeman.

Muller MJ, Klumpp S, Lipowsky R (2008). Tug-of-war as a cooperative mechanism for bidirectional cargo transport by molecular motors. Proc Natl Acad Sci USA 105, 4609–4614.

Pack-Chung E, Kurshan PT, Dickman DK, Schwarz TL (2007). A *Drosophila* kinesin required for synaptic bouton formation and synaptic vesicle transport. Nat Neurosci 10, 980–989.

Pilling AD, Horiuchi D, Lively CM, Saxton WM (2006). Kinesin-1 and dynein are the primary motors for fast transport of mitochondria in *Drosophila* motor axons. Mol Biol Cell 17, 2057–2068.

Ponti A, Vallotton P, Salmon WC, Waterman-Storer CM, Danuser G (2003). Computational analysis of F-actin turnover in cortical actin meshworks using fluorescent speckle microscopy. Biophys J 84, 3336–3352.

Reck-Peterson SL, Yildiz A, Carter AP, Gennerich A, Zhang N, Vale RD (2006). Single-molecule analysis of dynein processivity and stepping behavior. Cell 126, 335–348.

Saxton WM, Hicks J, Goldstein LS, Raff EC (1991). Kinesin heavy chain is essential for viability and neuromuscular functions in *Drosophila*, but mutants show no defects in mitosis. Cell 64, 1093–1102.

Schroer TA (2004). Dynactin. Annu Rev Cell Dev Biol 20, 759–779.

Shubeita GT, Tran SL, Xu J, Vershinin M, Cermelli S, Cotton SL, Welte MA, Gross SP (2008). Consequences of motor copy number on the intracellular transport of kinesin-1-driven lipid droplets. Cell 135, 1098–1107.

Simons M, Ikonen E, Tienari PJ, Cid-Arregui A, Monning U, Beyreuther K, Dotti CG (1995). Intracellular routing of human amyloid protein precursor: axonal delivery followed by transport to the dendrites. J Neurosci Res 41, 121–128.

Slemmon JR, Salvaterra PM, Crawford GD, Roberts E (1982). Purification of choline acetyltransferase from *Drosophila* melanogaster. J Biol Chem 257, 3847–3852.

Soppina V, Rai AK, Ramaiya AJ, Barak P, Mallik R (2009). Tug-of-war between dissimilar teams of microtubule motors regulates transport and fission of endosomes. Proc Natl Acad Sci USA 106, 19381–19386.

Spudich J (1990). Optical trapping: molecular molecules in motion. Nature 348, 284–285.

Stamer K, Vogel R, Thies E, Mandelkow E, Mandelkow EM (2002). Tau blocks traffic of organelles, neurofilaments, and APP vesicles in neurons and enhances oxidative stress. J Cell Biol 156, 1051–1063.

Stokin GB, Goldstein LSB (2006). Axonal transport and Alzheimer's disease. Annu Rev Biochem 75, 607–627.

Stokin GB *et al.* (2005). Axonopathy and transport deficits early in the pathogenesis of Alzheimer's disease. Science 307, 1282–1288.

Stone MC, Roegiers F, Rolls MM (2008). Microtubules have opposite orientation in axons and dendrites of *Drosophila* neurons. Mol Biol Cell 19, 4122–4129.

Svoboda K, Schmidt CF, Schnapp BJ, Block SM (1993). Direct observation of kinesin stepping by optical trapping interferometry. Nature 365, 721–727.

Szodorai A *et al.* (2009). APP anterograde transport requires Rab3A GTPase activity for assembly of the transport vesicle. J Neurosci 29, 14534–14544.

Theodoridis S, Koutroumbas K (2009). Pattern Recognition, 4th ed., Burlington, MA: Elsevier.

Tienari PJ *et al.* (1996). The beta-amyloid domain is essential for axonal sorting of amyloid precursor protein. EMBO J 15, 5218–5229.

Vallee RBV, Williams JCW, Varma D, Barnhar LE (2004). Dynein: an ancient motor protein involved in multiple modes of transport. J Neurobiol 58, 189–200.

Vaughan KT, Vallee RB (1995). Cytoplasmic dynein binds dynactin through a direct interaction between the intermediate chains and $p150^{Glued}$. J Cell Biol 131, 1507–1516.

Wang Z, Khan S, Sheetz MP (1995). Single cytoplasmic dynein molecule movements: characterization and comparison with kinesin. Biophys J 69, 2011–2023.

Wang Z, Sheetz MP (2000). The C-terminus of tubulin increases cytoplasmic dynein and kinesin processivity. Biophys J 78, 1955–1964.

Waterman-Storer CM, Holzbaur EL (1996). The product of the *Drosophila* gene, *Glued*, is the functional homologue of the $p150^{Glued}$ component of the vertebrate dynactin complex. J Biol Chem 271, 1153–1159.

Welte MA, Gross SP, Postner M, Block SM, Wieschaus EF (1998). Developmental regulation of vesicle transport in *Drosophila* embryos: forces and kinetics. Cell 92, 547–557.

Yamazaki T, Selkoe DJ, Koo EH (1995). Trafficking of cell surface beta-amyloid precursor protein: retrograde and transcytotic transport in cultured neurons. J Cell Biol 129, 431–442.

Yang G, Matov A, Danuser G (2005). Reliable tracking of large-scale dense particle motion for fluorescent live cell imaging. In: Proceedings of the 2005 IEEE Computer Society Conference on Computer Vision and Pattern Recognition (CVPR'05), Vol. 3, Washington, DC: Institute of Electrical and Electronics Engineers.

Yonekawa Y, Harada A, Okada Y, Funakoshi T, Kanai Y, Takei Y, Terada S, Noda T, Hirokawa N (1998). Defect in synaptic vesicle precursor transport and neuronal cell death in KIF1A motor protein-deficient mice. J Cell Biol 141, 431–441.